Identifying the possible driving mechanisms in Precipitation-Runoff relationships with nonstationary and nonlinear theory approaches

Li, Tongfang; Lan, Tian; Zhang, Hongbo; Sun, Jing; Xu, Chong Yu; David Chen, Yongqin

DOI
10.1016/j.jhydrol.2024.131535

Publication date
2024

Document Version
Final published version

Published in
Journal of Hydrology

Journal of Hydrology 639 (2024) 131535

Contents lists available at ScienceDirect

Journal of Hydrology

journal homepage: www.elsevier.com/locate/jhydrol

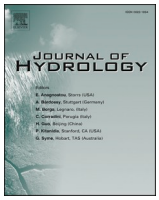

Research papers

Identifying the possible driving mechanisms in Precipitation-Runoff relationships with nonstationary and nonlinear theory approaches

Tongfang Li [a,b,c], Tian Lan [a,b,c,*], Hongbo Zhang [a,b,c], Jing Sun [d], Chong-Yu Xu [e], Yongqin David Chen [f]

[a] School of Water and Environment, Chang'an University, Xi'an 710054, China
[b] Key Laboratory of Subsurface Hydrology and Ecological Effects in Arid Region of the Ministry of Education, Chang'an University, Xi'an 710054, China
[c] Key Laboratory of Eco-Hydrology and Water Security in Arid and Semi-Arid Regions of Ministry of Water Resources, Chang'an University, Xi'an 710054, China
[d] Department of Intelligent Systems, Delft University of Technology, Van Mourik Broekmanweg 6, 2628 XE Delft, the Netherlands
[e] Department of Geosciences, University of Oslo, P.O. Box 1047Blindern, 0316 Oslo, Norway
[f] School of Humanities and Social Science, The Chinese University of Hong Kong, Shenzhen 518172, China

ARTICLE INFO

Keywords:
Precipitation-runoff relationships
Nonstationary
Nonlinear
Driving mechanisms
High-resolution hydrological model
Basin complexity

ABSTRACT

Climate change and complex anthropogenic activities have raised significant concerns regarding Precipitation-Runoff Relationships (PRR). Traditional methods, assuming stationary and linear conditions, often fail to adequately capture these intricate links. To address the limitations, we proposed an integrated framework, employing the Driving indices for Precipitation-Runoff relationships within the nonStationary and nonLinear theory approaches (DPRS and DPRL) to identify the possible driving mechanisms in PRR. The framework is validated across five sub-basins (WRB1-WRB5) within the Wei River Basin, known for its high spatiotemporal variability and intense anthropogenic activities. Spatiotemporal dynamics, nonstationary processes, and nonlinear interactions among various factors are assessed, including climate forcing, groundwater, vegetation dynamics, and anthropogenic influences. DPRS and DPRL assessments revealed that baseflow significantly influences PRR but with high uncertainty. Potential evapotranspiration plays a dominant role in driving negative PRR changes in WRB5 (weakening the correlation between precipitation and runoff), while vegetation dynamics negatively affect PRR with lower uncertainty. Anthropogenic influences represented by Impervious Surface Ratio (ISR), Night-Time Light (NTL), and population density (POP) exhibit varying driving levels, with ISR having the strongest and direct impact, closely linked to urbanization processes and scale within the study cases. The mutual validation of DPRS and DPRL confirms the dominance of baseflow in the Wei River Basin, with urbanization contributing to high ISR, NTL, and POP driving levels in WRB2 and WRB3. Afforestation policies intensify vegetation dynamics' impact in WRB4 and WRB5. This framework extends its utility to analyze various land evapotranspiration and soil moisture content at different depths in the PRR, supported by a physically-based hydrological model. Basin complexity is further employed to validate the reliability of the assessment outcomes. These insights contribute to a more comprehensive understanding of hydrological processes and facilitate informed decisions for sustainable water resource management within the basin.

1. Introduction

Precipitation is the source of runoff, and runoff is a lagged function of precipitation (Nourani et al., 2016; Saft et al., 2015; Zhang et al., 2018). It is important to understand the various properties of the interdependence of precipitation and runoff, as hydrologic models and decision frameworks rely on foundational assumptions and knowledge about this interdependence (Nourani et al., 2016; Saft et al., 2015; Zhang et al., 2018). For example, it is critical to represent the relationships between precipitation and runoff for predictive modeling (Ficklin et al., 2013; Hidalgo et al., 2009), reservoir and water resources decision-making (Hejazi and Cai, 2009; Hejazi et al., 2008; Quinn et al., 2017), as well as the preservation of ecosystem functionalities. The intricate dependencies of precipitation and runoff are filtered by characteristics such as basin size, topographical characteristics, soil composition, vegetation cover, and spatial heterogeneity (Bales et al., 2018). An

* Corresponding author.
E-mail address: tianlan@chd.edu.cn (T. Lan).

https://doi.org/10.1016/j.jhydrol.2024.131535
Received 5 November 2023; Received in revised form 7 April 2024; Accepted 3 June 2024
Available online 18 June 2024

increase in precipitation may directly lead to an increase in streamflow, but in the process of precipitation generating runoff, meteorological changes or anthropogenic interventions introduce diverse impacts on the runoff generation process. For instance, temperature-driven evaporation exerts a profound influence on runoff dynamics and its correlation with precipitation. In numerous regions, anthropogenic activities such as dam construction, urban impervious surfaces, agricultural practices, land-use changes, and other anthropogenic influences have modified historical or natural streamflow regimes. Consequently, the complex interplay of these intertwined processes has induced nonlinear and nonstationary patterns in regional streamflow behaviors (Dey and Mishra, 2017). These suggest a need for identifying the possible driving mechanisms of the Precipitation-Runoff Relationships (PRR) behind complicatedly nonlinear changes or nonstationary hydrological conditions.

Various methods have been employed to characterize the PRR with successful applications. The commonly utilized technique is the correlation coefficient method due to its simplicity and effectiveness. However, this method has certain limitations. Firstly, prior to using Pearson's correlation coefficient for assessing the PRR, prerequisites like the bivariate normality of the data must be met (Armstrong, 2019). However, the nonstationary characteristics of precipitation and runoff time series resulting from climate change, land conversion, and human water use challenge this assumption (Liu et al., 2015; Zhang et al., 2011b). Consequently, applying the correlation coefficient to detect PRR under nonstationary conditions is constrained. Additionally, the intricate interplay of climate change and anthropogenic activities impacts the water cycle across time scales (Abbott et al., 2019). Although Pearson's coefficient comprehensively reflects the PRR over a specific period, it fails to account for PRR in non-stationarity. Another common approach, the event runoff coefficient, quantifies retained precipitation in various storage components, such as vegetation interception, soil moisture accumulation, and percolation into deeper layers (Tarasova et al., 2018). While pivotal in estimating event runoff, the runoff coefficient has limitations. It yields anomalous values when precipitation is minimal, reflects integrated catchment characteristics, and relies on simplifications (Feng et al., 2016; Savenije, 1996). Hydrological modeling offers detailed insights into PRR through data-driven or process-based models (Nayak et al., 2013; Sikorska-Senoner and Quilty, 2021). However, these models demand substantial data. In addition, prevailing hydrological modeling approaches presuppose stationary climatic and catchment attributes (Pathiraja et al., 2016), which restricts their applicability in nonstationary environments. This may lead to model parameters being optimized to dynamic climatic and catchment conditions, potentially leading to a serious discrepancy between the simulated runoff and actual streamflow, thereby affecting water resources planning and operations. Some researchers have also conducted studies utilizing methodologies tailored for nonstationary environments. Zhang et al. (2015) employed the GAMLSS model to analyze flood frequency under both stationary and nonstationary conditions in the East River. Gu et al. (2017) developed GEV-CDN models considering time as a covariate to assess flood risk and failure risk of the major flood-control infrastructure in the Pearl River basin, China. Xie et al. (2019) proposed a hybrid model based "feature decomposition-learning reconstruction" named VMD-DBN-IPSO to improve the accuracy of short-term runoff forecasting. Substantial advancements have been achieved in flood research and runoff forecasting. To address the limitations inherent in the aforementioned techniques for PRR, Detrended Fluctuation Analysis (DFA) is considered, and it effectively examines power-law autocorrelations in nonstationary time series (Peng et al., 1994). Detrended Cross-Correlation Analysis (DCCA) detects power-law cross-correlations between nonstationary signals (Kantelhardt et al., 2002). Detrended Partial-Cross-Correlation Analysis (DPCCA) further eliminates the impact of other signals on the two examined signals, revealing the intrinsic cross-correlations between them (Yuan et al., 2015). Building upon DCCA and DPCCA, we propose an index that overcomes the above limitations, offering a robust measure of the influence on PRR, independent of data sequence lengths and catchment types. The index evaluates driving levels and directions, accounts for characterizing uncertainties, considers the linear aspects of the time lag associated with baseflow, and contributes to a comprehensive understanding of nonstationary PRR scenarios.

Entropy, a fundamental concept with wide-ranging applications across engineering and scientific disciplines, serves to characterize the inherent disorder within systems or information, thereby providing valuable insights into challenges related to information processing, uncertainty assessment, and risk analysis (Mishra and Ayyub, 2019). Shannon entropy (Shannon, 1948) quantifies the expected information within messages (Wu et al., 2013), which found utility in various domains, including electrical engineering, statistics, mathematics, statistical physics, and thermodynamics (Aguiar and Guedes, 2015; Lin and Ho, 2015; Perugini et al., 2015). Information Theory (IT) is based on Shannon Entropy (Shannon, 1948) and has found application in numerous hydrology-related investigations focusing on the analysis of spatiotemporal variability of precipitation, streamflow, precipitation deficit, and flow modeling (Brunsell, 2010; Chen et al., 2007; Mishra et al., 2009). Pechlivanidis et al. (2016) introduced an importance-weighted entropy-based measure to counter the tendency of common binning approaches to over-emphasize information contained in the low flows that dominate the record. The measure used a novel binning method and overcame artefacts due to data resolution and undersampling. Sang et al. (2018) employed the Shannon entropy index to investigate the spatiotemporal variability of meteorological droughts over China. Compared with SPEI, the entropy index had an explicit definition and meaning and was much easier to calculate. More importantly, it reflects the physical formation process of droughts, so the proposed entropy index is an effective index to evaluate droughts. Goodwell et al. (2020) applied information measures to binary sequences of precipitation occurrence to quantify uncertainty and predictability in the form of lagged mutual information between the current state and two time-lagged histories, as well as associated dominant time scales. Franzen et al. (2020) employed information theory-based measures to detect thresholds, timescales, and strengths of daily precipitation influences on downstream flows in the Colorado Headwaters. Notably, entropy serves as a quantifiable metric for assessing signal uncertainty, simultaneously enabling the computation of mutual information between signal pairs. Mutual information (MI) is a measure of interdependence between variables (Cover, 1999). In these regards, we applied MI to develop an index for identifying the possible driving mechanisms in PRR using a nonlinear theory approach. By calculating mutual information between driving factors and precipitation (runoff), this approach quantifies the nonlinear nature of their associations. Higher mutual information values signify stronger associations or interdependencies.

According to the quantification analysis of driving factors influencing the PRR, a comprehensive understanding of the controlling processes in the PRR within nonstationary and nonlinear environments is crucial for effective water management and adapting to changing conditions (John et al., 2022). Diverse factors influence the PRR across various time scales (Liu et al., 2019). Regional and global climate patterns significantly affect PRR, where the spatial–temporal distribution of precipitation, driven by atmospheric circulation, impacts runoff timing and magnitude. Anthropogenic climate change intensifies extreme weather events (Konapala et al., 2020). Natural catchment characteristics like size, shape, slope, and geology significantly influence the PRR. Steep slopes and impermeable surfaces lead to rapid surface runoff during heavy rainfall (van Rensch et al., 2023). Human-driven land use changes, including deforestation, urbanization, agriculture, and land reclamation, alter hydrological responses, contributing to increased surface runoff, reduced infiltration, and modified runoff patterns (Kayitesi et al., 2022). Soil properties such as porosity, permeability, and moisture influence precipitation partitioning into infiltration and runoff.

Soil moisture levels directly impact runoff during rainfall (Western et al., 1999). Vegetation's role in the water cycle, particularly evapotranspiration, affects runoff proportions. Changes like deforestation or afforestation alter the runoff-evaporation balance (Bai et al., 2020). Anthropogenic activities such as water abstraction, reservoir operations, and irrigation directly influence runoff timing and magnitude, further affecting the PRR. Hydrological infrastructure like dams and stormwater systems alter flow pathways and impact runoff generation (Wang et al., 2022). Accordingly, the intricate interplay of these driving factors manifests in the complexity of the PRR, necessitating a comprehensive understanding of effective water resource management and adaptation strategies in the face of evolving environmental conditions.

The primary aim of this study is to employ nonstationary and nonlinear theory approaches to quantify the relative importance of driving factors that exert influence over the precipitation-runoff relationships. It seeks to identify the possible driving mechanisms in the dependencies between precipitation and runoff, particularly within regions subjected to anthropogenic disturbances. These insights are pivotal in enabling informed decision-making for the sustainable management of water resources within a given catchment. The paper focuses on the following three aspects:

- A Driving index for Precipitation-Runoff relationships with the nonStationary theory approach (DPRS) is proposed to identify the driving levels and directions under nonstationary circumstances.
- A Driving index for Precipitation-Runoff links with the nonLinear theory approach (DPRL) is further developed based on mutual information techniques to quantify the nonlinear nature of their associations.
- Following the quantitative assessment of candidate influencing factors in the precipitation-runoff relationships within nonstationary and nonlinear hydrological processes, the possible driving mechanisms for these relationships are investigated based on diverse catchment response elements.

To achieve the above aims, this study took five sub-basins with different catchment characteristics in the Wei Basin River to demonstrate our research objective and methods. The remainder of the paper is organized as follows: Section 2 analyses the research basins. Section 3 introduces the methods. The key results and discussion are presented in Sections 4 and 5. Section 6 exhibits the main conclusions and future research of this study.

2. Data description and analysis

2.1. Data description

The Wei River Basin, situated between 103°05′E–110°05′E, 33°50′N–37°05′N, is the Yellow River's primary tributary in China (refer to Fig. 1a). Spanning an area of 134,800 km2, it runs 818 km in length (Huang et al., 2017b). Characterized by a continental monsoon climate, this basin has high variability in its dry and wet periods. Precipitation predominantly occurs between June and October, with an average annual precipitation of 572 mm. The basin's average temperature is approximately 10.6℃, and its annual runoff is about 60 mm (Zhao et al., 2015). Serving as a significant agricultural center in Northwest China, the Wei River Basin grows grains to meet the water needs of 22 million residents. Economically, it greatly contributes to the Guanzhong-Tianshui Economic Zone. Over the past fifty years, anthropogenic interventions—including agricultural irrigation, reservoirs, sediment-trap dams, river diversions, and soil conservation—have significantly influenced hydrological processes in the basin (Chen et al., 2016; Zuo et al., 2012). Such activities have caused a significant decrease in annual streamflow (Zhang et al., 2022), challenging the basin's previously assumed hydrological stationarity, and amplifying the complexity and nonlinear characteristics of the basin. Given this, the Wei River Basin is an ideal region for exploring precipitation-runoff interactions within a nonstationary and nonlinear hydrological system. This study employs data from five sub-basins (WRB1-WRB5) to highlight varying precipitation-runoff characteristics and degrees of anthropogenic intervention managed by hydrological monitoring stations at Qinan, Weijiabao, Xianyang, Zhangjiashan, and Zhuangtou (Fig. 1a). They represent various locations, involving the upstream, middle sections, and the two primary tributaries in the downstream: the Jing and Beiluo

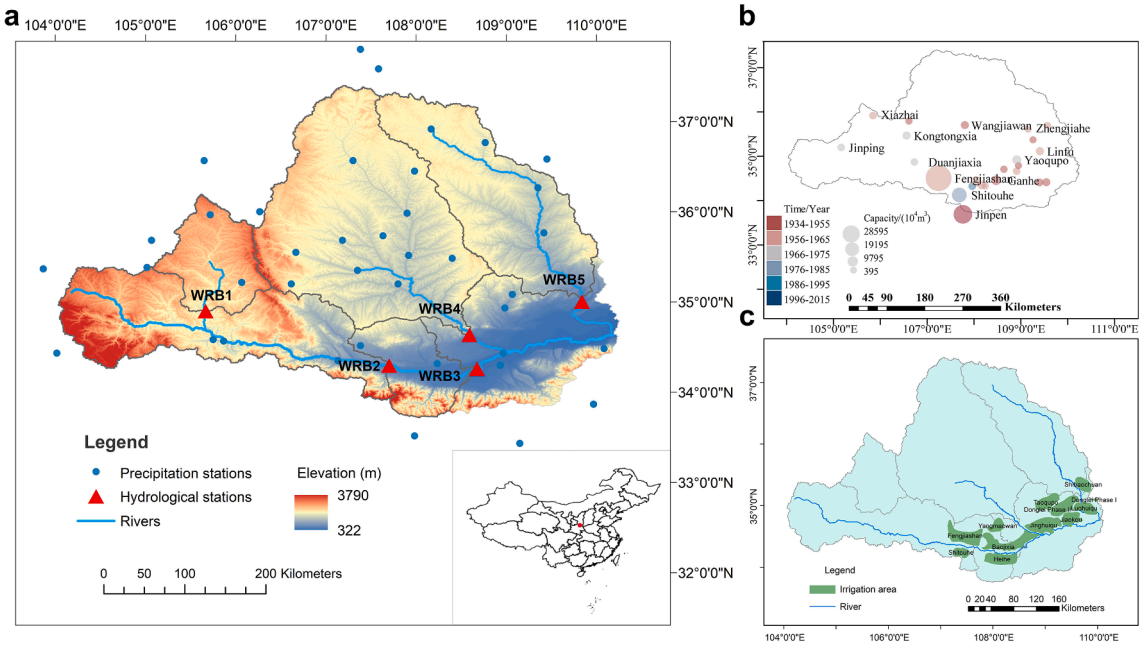

Fig. 1. A, information of the study area, including the five selected sub-basins (wrb1, wrb2, wrb3, wrb4, and wrb5), hydrological monitoring stations, and a meteorological station (referred to as precipitation stations) within the wei river basin. in the lower right section of the figure, a red circle indicates the geographical location of the wei river basin in china. b, completion time and storage capacities of the main reservoirs in the wei river basin. c, location of irrigation districts in the economic core of the wei river basin. (For interpretation of the references to colour in this figure legend, the reader is referred to the web version of this article.)

Rivers.

For a comprehensive understanding of the precipitation-runoff dependencies within a changing environment, this study utilizes various datasets, including observed streamflow, meteorological records, geographic data, and remote sensing datasets indicative of anthropogenic influences. Daily streamflow data are sourced from the Yellow River Conservancy Commission (Table S1), which details the drainage areas, durations, and geographical coordinates of hydrological monitoring stations. The Chapman-Maxwell filter method, elaborated upon in Supporting Information S2, was employed to compute the daily baseflow (*BF*). Daily meteorological records from 1960 to 2019 were obtained from the China National Surface Weather Station (V3.0) (http://www.nmic.cn/). Potential evapotranspiration (ET_0) was calculated using the Penman-Monteith equation, elaborated upon in Supporting Information S2. Elevation data at a 90 m resolution were sourced from the USGS Shuttle Radar Topography Mission (SRTM) (http://srtm.csi.cgiar.org/). Global Inventory Modelling and Mapping Studies (GIMMS) NDVI3g dataset with a spatial resolution of 1/12° are utilized to assess vegetation cover dynamics from 1982 to 2014 (https://ecocast.arc.nasa.gov/data/pub/gimms/3g.v1/). Impervious Surface Ratio (ISR) data were from 1985 to 2019 at a spatial resolution of 30 m were used to gauge urbanization rates (Gong et al., 2020). Additionally, Night-Time Light (NTL) data from 1992 to 2019 at a spatial resolution of 30-arc seconds served as a metric for evaluating diverse anthropogenic and environmental footprints (Ceola et al., 2014). Population data (POP) from 2000 to 2019 at a resolution of 30 arc seconds were procured from WorldPop (WorldPop, 2018), offering insights into population distribution and migration. Missing data within records are imputed through interpolation techniques utilizing observational data obtained from adjacent stations. Spatial data is acquired through area-weighted aggregation of site-specific data within the region, employing methods such as the Thiessen polygon technique or extraction from remote sensing datasets. The raster data utilized in the hydrological model is standardized to a resolution of 1 km, with adjustments made through resampling for datasets failing to meet the requisite resolution standards. Meteorological data at a 1-kilometer resolution is derived from interpolating meteorological station observation data using the Kriging interpolation method.

This study further investigates the anthropogenic influence, specifically reservoirs and their corresponding large-scale irrigation areas, which are pivotal in influencing the Wei River Basin's water cycle. Data from the Yellow River Conservancy Commission are utilized. The reservoirs affected the PRR in the Wei River Basin due to extensive surface water withdrawals for agricultural irrigation purposes (Zhan et al., 2014). Notably, the Wei River Basin's primary reservoirs are closely linked to corresponding irrigation districts, with district sizes proportionate to reservoir scales. Therefore, reservoir construction not only alters the seasonal water discharge within a given year but also significantly modifies inter-annual distribution. Data collection challenges led us to primarily rely on reservoir construction dates and capacities (Fig. 1b) to assess their PRR impact. In WRB1, the Xiazhai Reservoir, a small-scale facility, was built in the 1970 s. In WRB2, the largest reservoir in the Wei River Basin, Fengjiashan Reservoir, was constructed in 1974. A cluster of large-capacity reservoirs and their associated irrigation districts (Fig. 1c) are evident between WRB2 and WRB3, including Zhangjiazuitou Reservoir, Shitouhe Reservoir, Xinyigou Reservoir, Yangmaowan Reservoir, Dabeigou Reservoir, Laoyaju Reservoir, and Shibianyu Reservoir, mostly built concurrently around the early 1970 s. In WRB4, the Xijiao Reservoir, with a large-scale irrigation district, was established in 1997, directly influencing downstream streamflow at the Zhangjiashan hydrological monitoring station. WRB5 features Zhengjiahe Reservoir and Linfu Reservoir, both with minor capacities, built in the 1970 s. Additionally, a large-scale irrigation area downstream of WRB5, regulated by the Shibaochuan Reservoir, impacts streamflow at the Zhuangtou hydrological station.

2.2. Data analysis

2.2.1. Possible driving factors

The PRR under nonstationary and nonlinear circumstances is possibly controlled by climate forcing, groundwater, vegetation dynamics, and anthropogenic influences (Fig. 2b).

Climate forcing: Potential evapotranspiration (ET_0) is regarded as a representative climate-driving factor influencing PRR. This is because ET_0 is regulated by various atmospheric parameters under anticyclonic conditions, including air temperature, heat flux, wind speed, saturated vapor pressure, net radiation, and relative humidity (Hobbins et al., 2016; Liu et al., 2020). For instance, higher temperatures generally lead to increased evapotranspiration, while high humidity limits evaporation due to abundant moisture in the air. Increased wind speed accelerates evaporation by facilitating the departure of water molecules from the surface. Extended hours of sunshine contribute to surface energy input, thereby promoting water evaporation. However, changes in these atmospheric parameters associated with ET_0 may not necessarily result in corresponding variations of changes in actual evapotranspiration (AET). This is because AET may often be limited by water availability rather than energy, leading to an unclear net effect of AET changes on PRR (Saft et al., 2015).

Groundwater: Groundwater, characterized by its large water storage capacity and long-term memory, plays a crucial role in PRR (Carlier et al., 2018). Contributions of shallow and deep groundwater inflows to streamflow exhibit distinct response time scales (Hare et al., 2021). For instance, streamflow can be attributed to shallow inflow processes, such as perched saturation along hydraulic gradient fronts, displaying transient behavior with short response times (ranging from days to weeks) (Hirmas et al., 2018). In contrast, discharge from confined aquifers exhibits slower dynamics, including trends spanning multiple years. Furthermore, groundwater interactions extend beyond catchment boundaries, influencing groundwater quantity through hydraulic gradients and regulating the exchange between regional groundwater and surface water (Bouaziz et al., 2018; Fowler et al., 2020). Additionally, anthropogenic impacts on groundwater extend to affect surface water runoff, including groundwater extraction, and modifications in vadose zone thickness (Fowler et al., 2022).

Vegetation dynamics: Vegetation interacts with the PRR through processes such as evapotranspiration, interception, infiltration, and groundwater recharge (Ajami et al., 2017). Conversely, changes in precipitation patterns, rising temperatures, and variations in water availability directly impact vegetation growth and transpiration. In recent decades, afforestation programs have been proposed to harness benefits related to flood mitigation and carbon storage. The impact of afforestation on streamflow across diverse catchments is found to consistently decrease median and low streamflow (Buechel et al., 2022). Hence, the investigation of vegetation dynamics is considered a candidate driving factor for PRR.

Anthropogenic influences: Intensified anthropogenic activities, linked to urbanization and population growth, threaten global water resource sustainability (Mekonnen and Hoekstra, 2016). Gathering continuous and long-term data on anthropogenic impacts related to the water cycle and human activities at the catchment level presents challenges (Thorslund and van Vliet, 2020). Remote sensing provides valuable tools for analyzing global human impacts on river systems, identifying human pressures, and assessing their temporal and spatial distribution (Ceola et al., 2019). The influence of anthropogenic factors on precipitation-runoff relationships is multifaceted and intricate. Three factors were selected for comprehensive examination in this study to elucidate the impacts of anthropogenic influences on precipitation-runoff relationships. Impervious surfaces, consisting of artificial structures obstructing natural water infiltration, are key components of urban settlements (Gong et al., 2020). High Impervious Surface Ratio (**ISR**) in urbanized areas affects surface energy and water balance, influencing extreme precipitation and floods (Lu et al., 2019). Changes in ISR impact

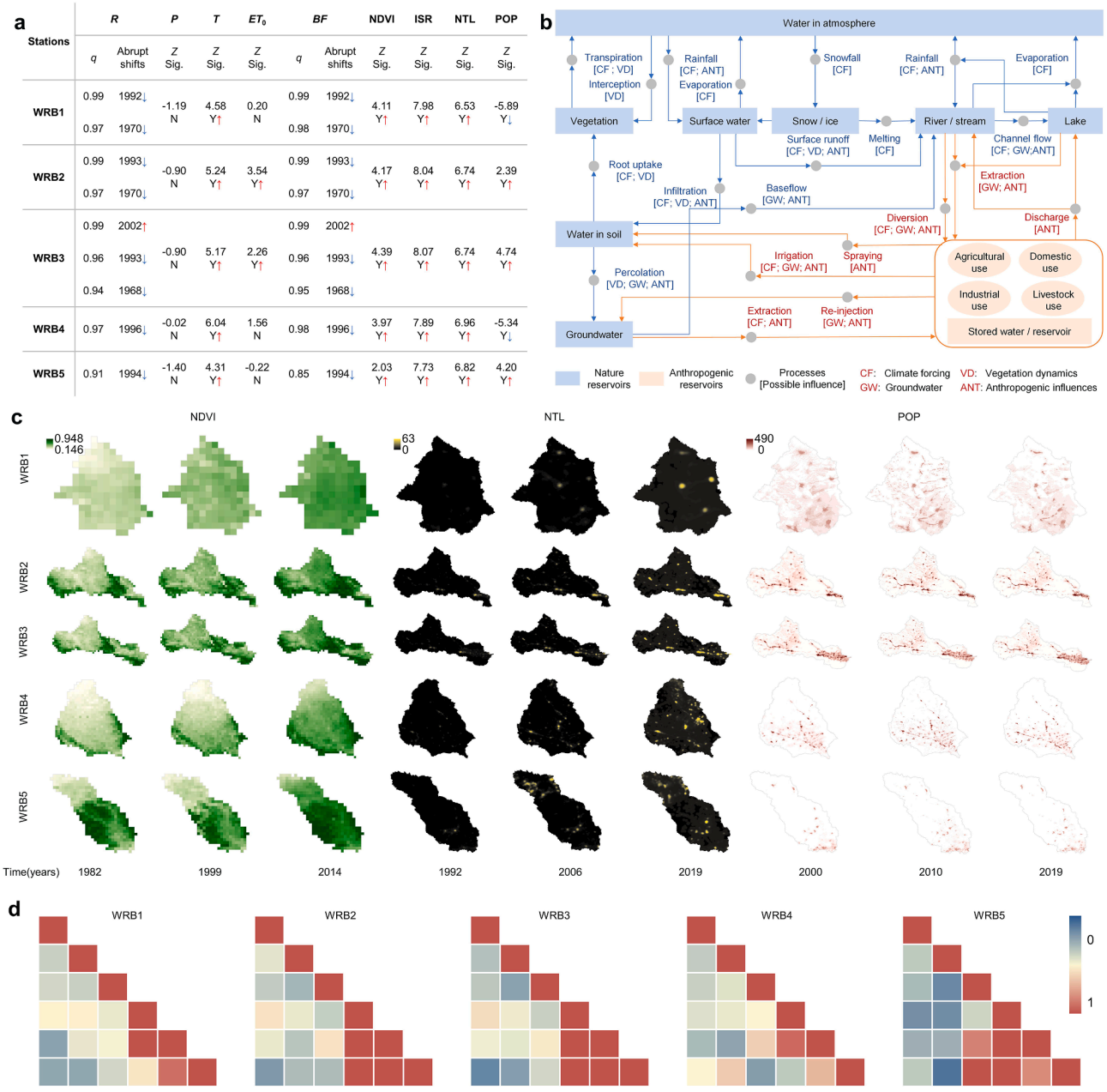

Fig. 2. a, Nonstationarity analysis results for hydrological process datasets (an upward arrow symbolizes an increasing trend within the data series, while a downward arrow signifies a decreasing trend; the designation Y denotes a statistically significant change trend, whereas N indicates a lack of statistical significance in the labeled change trend). **b,** Visual synthesis of selected process explanations for possible driving mechanisms in PRR under nonstationary and nonlinear processes, depicting a general catchment affected by complex anthropogenic interference. **c,** Remote sensing images characterizing anthropogenic influences. **d,** Heatmap for interconnection of the nonlinear relationships (MIC values) among the candidate driving factors. The factors studied are ET_0, *BF*, NDVI, ISR, NTL, and POP (from top to bottom, left to right).

the PRR through four mechanisms: (1) Increased ISR raises surface runoff, elevating flood risk and transporting pollutants to water bodies. (2) ISR reduces soil water infiltration, enhancing surface moisture retention and affecting soil water availability and hydrological processes. (3) The expansion of ISR decreases groundwater recharge. Assuming that preferential flow occurs in specific areas of a catchment, the increase in the ISR not only blocks the infiltration process but also disrupts the preferential flow process. Hence, expanding the ISR reduces groundwater recharge by affecting both infiltration and preferential flow processes (Shuster et al., 2005). Night-Time Light (**NTL**) products provide comprehensive insights into human presence and economic development's influence on water resources (Ceola et al., 2019). NTL affects the PRR through two mechanisms: (1) NTL's heat emission increases urban temperature, impacting the regional hydrological cycle by enhancing convection and influencing precipitation formation and distribution (Liao et al., 2017). It also raises localized evaporation, reducing surface runoff and precipitation infiltration. (2) NTL reflects urbanization and economic development, indicating increased impervious surfaces and water usage, disrupting infiltration, recharge, and post-precipitation evaporation (Elvidge et al., 2007). Higher population densities (**POP**) in regions often result in increased urbanization and more impermeable surfaces like buildings and roads. The impact on the PRR can be understood through three key aspects. (1) Higher population densities lead to greater water demand for domestic, industrial, and agricultural purposes, affecting natural flow patterns and water availability (Fang and Jawitz, 2019). (2) As population densities rise, there is

a greater need for infrastructure, urbanization, and agricultural expansion, which alter the landscape, affecting the hydrological cycle (Hobeichi et al., 2022). (3) In densely populated regions, excessive groundwater extraction can deplete resources, leading to reduced water availability and land subsidence (Fang and Jawitz, 2019).

2.2.2. Spatiotemporal analysis of driving factors

From a spatiotemporal perspective (see Fig. 2c), the Hulu River Basin (WRB1) is situated in the upper reaches of the Wei River Basin. This sub-basin experiences minimal anthropogenic impact on its river system. The southern section of the sub-basin, near the Liupan Mountains and Long Mountains, is covered by thick forests and high vegetation characteristics. The implementation of ecological conservation projects (Han et al., 2020), such as the soil and water conservation project, has resulted in an annual increase in NDVI values across the sub-basin (see Fig. 2a). NTL and POP values in the WRB1 are relatively low compared to other sub-basins, with their spatial distribution increasing from the northwest to the southeast. Especially, the NTL values showed a sharp increase after 2000 due to urban construction expansion in this sub-basin. However, the population density decreased primarily due to rural-to-urban migration (Huang et al., 2014). Although satellite images of ISR have a similar spatial distribution to the NTL image, they are not visible in Fig. 2 due to their reduced form. Hence, the changes in ISR are only analyzed in the temporal dynamics here. The WRB2 is situated in the middle reaches of the Wei River Basin, passing through Tianshui and Baoji cities. This sub-basin is characterized by a high level of population density and urbanization level (Zuo et al., 2015). NTL and POP values are concentrated in the two urban areas, with Baoji City, situated downstream, exhibiting higher NTL and POP values than Tianshui City, located upstream. After 2000, the ISR and NTL values in the sub-basin displayed a significant increase, while the overall POP values increased but had a decreasing trend after 2014. Vegetation coverage spatially increases from the northwest to the southeast and shows an annual increasing trend over time. WRB3 flows through Xianyang City, known for its robust economic performance, high level of urbanization, and dense population (Yang et al., 2020). The downstream urban agglomeration exhibits prominently high values of NTL, ISR, and POP, concentrated in specific spatial locations. Moreover, the spatial distribution and temporal variation of NDVI values exhibit similarities to those observed in WRB2 (Yang et al., 2020). WRB4 flows through the cities of Qingyang City and Pingliang City. The river also runs through the Zhangjiashan Reservoir, primarily utilized to abstract water for agricultural irrigation. (Zhang et al., 2019), directly regulating the river's annual discharge. The sub-basin's northern section is positioned in the gully terrain of the Loess Plateau, while the southern part lies in the Guanzhong Plain. Consequently, the NDVI values display a spatial increase from north to south. NTL and POP values also exhibit a corresponding rise from north to south, mainly concentrating in the southern Guanzhong Plain. With the development of urban construction, ISR and NTL values have increased annually. However, POP values have gradually declined, primarily due to population migration to the adjacent city of Xi'an, the largest core city in the Wei River Basin. WRB5 is comparatively less impacted by anthropogenic activities (Gao et al., 2013). The spatial distribution of NDVI, NTL, ISR, and POP values displays an incremental rise from north to south, with a corresponding annual increase over time.

2.2.3. Nonstationary analysis of driving factors

Mean and trend are essential statistical properties that remain constant over time in stationary conditions and are typically utilized to identify abrupt shifts and gradual changes in nonstationary conditions, respectively (Cryer and Kellet, 1991). We used the Pettitt test with Trend-Free Pre-Whitening and Binary Segmentation (TFPW-BS-Pettitt) to find abrupt shifts in runoff and baseflow. TFPW mitigates autocorrelation effects (Yue et al., 2003). The Binary Segmentation (BS) method (Lee and Verma, 2012) identifies multiple abrupt shift points iteratively. The non-parametric Mann-Kendall (MK) test assesses trends (Yue and Wang, 2004), with autocorrelation removed using TFPW before the MK test. Detailed calculations are in Supporting Information S3. Fig. 2a presents nonstationary testing results for hydrological datasets. The TFPW-BS-Pettitt method identified significant abrupt time points for runoff in WRB1, WRB2, WRB3, WRB4, and WRB5, occurring in 1992, 1993, 2002, 1996, and 1994, respectively. Baseflow showed similar significant abrupt shift points in the sub-basins. The possible reason is that the Wei River Basin is situated in a semi-arid region where streamflow is primarily influenced by groundwater (Zhao et al., 2015). Precipitation time series showed non-significant trends, but temperature and potential evapotranspiration exhibited significant upward trends in some sub-basins. These changes may be attributed to the combined effects of global warming, urban expansion, and regional climate processes (Huang et al., 2021). The NDVI values have increased significantly due to soil and water conservation projects since the 1950 s (Chen et al., 2007). Satellite data, including ISR, NTL, and POP, representing human pressure on the river system showed an overall upward trend, reflecting urbanization and increased human activities in the Wei River Basin (Chang et al., 2015).

2.2.4. Nonlinear interactions among driving factors

The Maximal Information Coefficient (MIC) metric measures nonlinear correlations among driving factors (Fig. 2d) (Zhang et al., 2014). The heatmap analysis shows significant nonlinear correlations among the anthropogenic-related driving factors (POP, NTL, ISR) in the five sub-basins. However, the correlation between POP and ISR is weak in WRB1 and WRB4, likely due to rural-to-urban migration. Baseflow has weak correlations with other factors, and potential evapotranspiration also exhibits relatively weak correlations, possibly due to integrated climate forcing effects at global and regional scales. In WRB5, NDVI shows strong associations with POP, NTL, and ISR, likely due to simultaneous soil and water conservation and urbanization processes in this sub-basin.

3. Methods

To gain insight into the possible driving mechanisms affecting the Precipitation-Runoff Relationships (PRR) within nonstationary and intricate nonlinear hydrological processes, we have developed innovative indices referred to as the Driving indices for Precipitation-Runoff relationships with the nonStationary and nonLinear theory approach (DPRS and DPRL). The indices serve as tools for evaluating driving levels and directions that influence PRR, which effectively address the limitations of conventional approaches used to characterize PRR and their driving mechanisms within nonstationary and nonlinear systems. The investigation into the candidate driving factors influencing PRR includes climate forcing, groundwater, vegetation dynamics, and anthropogenic influences. The anthropogenic influence factors are derived from long-term continuous series of remote sensing data, categorized at the catchment scale. The spatiotemporal dynamics, nonstationary processes, and nonlinear interactions among the factors were first assessed. By incorporating the driving levels and directions of driving factors computed from DPRS and DPRL, the plausible process explanations for influencing PRR in the study cases were deduced. Furthermore, the DPRS and DPRL indices are applied to analyze the driving mechanisms governing various land evapotranspiration and soil moisture content at different depths in the PRR using a physically-based hydrological model. In addition to the mutual validation of the DPRS and DPRL indices, the concept of basin complexity is further employed to validate the reliability of the assessment outcomes derived from these two indices. The overall framework is visually illustrated in Fig. 3.

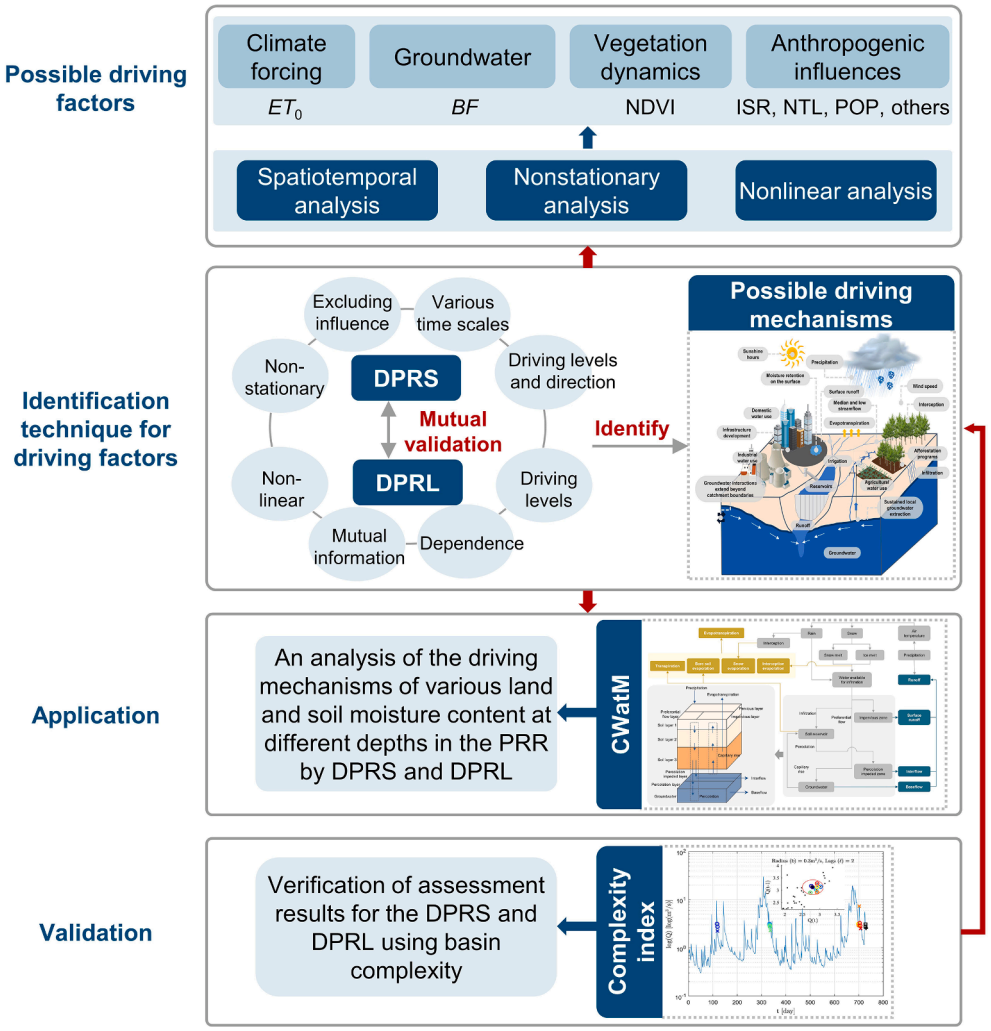

Fig. 3. Illustration of the framework for identifying the possible driving mechanisms in precipitation-runoff relationships with nonstationary and nonlinear theory approaches.

3.1. Identification technique for driving factors with nonstationary theory approach

A Driving index for Precipitation-Runoff relationships with the nonStationary theory approach (DPRS) is proposed to identify the possible driving mechanisms that influence the precipitation-runoff connections within nonstationary hydrological processes. This index overcomes the limitations of conventional approaches used to describe PRR and their driving mechanisms under nonstationary conditions. The calculation procedure for the DPRS index is as follows.

Step 1: The time lag between precipitation and baseflow is given by,

$$R(m) = \sum_{i=1}^{N} x_i^{\mathrm{Pre}} x_{i-m}^{\mathrm{BF}} \tag{1}$$

The $R(m)$ is the cross-correlation coefficient which is calculated by the XCORR function; m is the time lag, and its range is [-12, 0], which was selected based on the monthly time scale; x_i^{Pre} is precipitation time series (i = 1, 2, 3, …,N); x_{i-m}^{BF} represents the baseflow time series, where x_{i-m}^{BF} is equal to zero when $i - m$ exceeds N.

$$R(m_{\max}) = \max\{R(m)\} \tag{2}$$

where $m_{\max}$ corresponds to the time lag m at which $R(m)$ achieves its maximum value.

$$\begin{cases} x_i^{\mathrm{BF\_lag}} = x_{i-m_{\max}}^{\mathrm{BF}} & i - m_{\max} \le N \\ x_i^{\mathrm{BF\_lag}} = x_N^{\mathrm{BF}} & i - m_{\max} > N \end{cases} \tag{3}$$

where $x_i^{\mathrm{BF\_lag}}$ denotes the baseflow time series at the time lag of $m_{\max}$.

Step 2: Suppose that the precipitation time series, runoff time series, and the influencing factor of PRR are $\{x_i^1\}$, $\{x_i^2\}$, $\{x_i^3\}$ (i = 1, 2, 3, …,N), respectively. Each time series $\{x_i^j\}$ (j = 1, 2, 3) is accumulated as the profile $\{P_k^j\}$ (k = 1, 2, 3).

$$P_k^j = \sum_{i=1}^{k} x_i^j \tag{4}$$

Step 3: The profiles are divided into $N - s + 1$ overlapping sub-periods. The value range of s needs to be selected according to the research purpose. The value range in this study is [36, N-1]. The time nodes of each sub-period h are from h to $h + s - 1 (h = 1, \cdots, N - s + 1)$. Then, the local trend $\{\widetilde{P_{k,h}^j}\}$ is generated by a least-squares polynomial fitting. Accordingly, the detrended residual series $\{Y_{s,l}^j\}$ ($l = (h-1)\hat{A}\cdot s + k - h + 1$) are calculated by the difference between the original time series and the local trend.

$$Y_{s,l}^j = P_k^j - \widetilde{P_{k,h}^j} \tag{5}$$

Step 4: The cross-correlation levels $\rho_{j_1 j_2}(s)$ between any two time series on the time scales of s are estimated, which ranges from −1 to 1. The $\rho_{j_1 j_2}(s)$ is also referred to as the DCCA (Detrended Cross-Correlation Analysis) index, which characterizes the PRR under nonstationary hydrological processes. The coefficients matrix is constituted as,

$$\mathrm{DCCA}(s) = \rho_{j_1 j_2}(s) = \frac{\sum_{l=1}^{(N-s+1)\hat{A}\cdot s} Y_{s,l}^{j_1} Y_{s,l}^{j_2}}{\sqrt{\sum_{l=1}^{(N-s+1)\hat{A}\cdot s} Y_{s,l}^{j_1} Y_{s,l}^{j_1}} \sqrt{\sum_{l=1}^{(N-s+1)\hat{A}\cdot s} Y_{s,l}^{j_2} Y_{s,l}^{j_2}}} \tag{6}$$

$$\rho(s) = \begin{bmatrix} \rho_{1,1}(s) & \rho_{1,2}(s) & \rho_{1,3}(s) \\ \rho_{2,1}(s) & \rho_{2,2}(s) & \rho_{2,3}(s) \\ \rho_{3,1}(s) & \rho_{3,2}(s) & \rho_{3,3}(s) \end{bmatrix} \tag{7}$$

Step 5: The partial-cross-correlation level $\rho(1,2;s)$ between the precipitation and runoff is determined based on the inverse matrix of $\rho(s)$ which is defined as,

$$C(s) = \rho^{-1}(s) = \begin{bmatrix} C_{1,1}(s) & C_{1,2}(s) & C_{1,3}(s) \\ C_{2,1}(s) & C_{2,2}(s) & C_{2,3}(s) \\ C_{3,1}(s) & C_{3,2}(s) & C_{3,3}(s) \end{bmatrix} \tag{8}$$

$$\rho(1,2;s) = \frac{-C_{1,2}(s)}{\sqrt{C_{1,1}(s) C_{2,2}(s)}} \tag{9}$$

Step 6: The $\rho_{1,2}(s)$ denotes the PRR on the time scales of s with nonstationary effects removed. The $\rho(1,2;s)$ characterizes the cross-correlation between precipitation and runoff by eliminating the influences of an external factor. The difference between $\rho_{1,2}(s)$ and $\rho(1,2;s)$ represents the driving level of an influencing factor on PRR. To address the issue of inconsistent data-sequence lengths among different driving factors within a catchment and facilitate comparisons between different catchments, we introduce the concept of relative error. It is computed by dividing the difference between $\rho_{1,2}(s)$ and $\rho(1,2;s)$ by $\rho_{1,2}(s)$. The $\rho_{1,2}(s)$ represents the specific PRR of a catchment at a given time scale s, reflecting the catchment-properties PRR influenced by integrated multifactorial forces. However, when the denominator $\rho_{1,2}(s)$ approaches zero, there is a risk of encountering abnormally high values in the DPRS index. To address this, we update the denominator to $\rho_{1,2}(s) + 1$. Notably, a positive value of the DPRS index signifies that the driving factor positively enhances the P-R link, while a negative index value suggests a negative effect of the driving factor on the P-R link. The calculation of the DPRS index is given by,

$$\mathrm{DPRS}(1,2;3;s) = \frac{\rho_{1,2}(s) - \rho(1,2;s)}{\rho_{1,2}(s) + 1} \tag{10}$$

Step 7: The above formula for DPRS can only provide index values across time scales. However, we prefer a definitive measure within a given period. Hence, the kernel density function is utilized.

$$\widehat{f}_w(\mathrm{DPRS}) = \frac{1}{(b-a+1)w} \sum_{s=a}^{b} K\left(\frac{\mathrm{DPRS} - \mathrm{DPRS}(1,2;3;s)}{w}\right) \tag{11}$$

$$\widehat{f}_w(\mathrm{DPRS}_{\max}) = \max\{\widehat{f}_w(\mathrm{DPRS})\} \tag{12}$$

where $\widehat{f}_w(\mathrm{DPRS})$ represents the kernel density function with w which denotes the bandwidth. The range of s is set as $[a, b]$, and a GridSearchCV is conducted for the optimal range (Pedregosa et al., 2011). The search space for s is set to [0.05, 1.95] with a step size of 0.05. $K(.)$ denotes the kernel function. $\mathrm{DPRS}_{\max}$ corresponds to the maximum value of kernel density for DPRS. Here, the Gaussian kernel density function is utilized for estimating kernel density.

$$K(x) = \frac{1}{\sqrt{2\pi}} \exp\left(-\frac{1}{2}x^2\right) \tag{13}$$

3.2. Identification technique for driving factors with nonlinear theory approach

Furthermore, a Driving index for Precipitation-Runoff links with the nonLinear theory approach (DPRL) is developed based on mutual information technique to quantify the nonlinear nature of their associations. The calculation procedure for the DPRL index is as follows.

Step 1: Involve three time series: the runoff time series denoted as X_t, the precipitation time series denoted as Y_t, and an influencing factor denoted as Z_t, where $t = 1, 2, \cdots, n$, and n signifies the length of the time series. The initial computation entails deriving the cumulative frequency for each time series. Subsequently, the runoff time series is transformed into the following time series Q_t:

$$Q_t = \begin{cases} 1, & X_t \le X^{20} \\ 2, & X^{20} < X_t \le X^{40} \\ 3, & X^{40} < X_t \le X^{60} \\ 4, & X^{60} < X_t \le X^{80} \\ 5, & X_t > X^{80} \end{cases} \tag{14}$$

where X^{20}, X^{40}, X^{60}, and X^{80} correspond to X_t when the cumulative frequencies are 20 %, 40 %, 60 %, and 80 %, respectively. Similar processing is applied to the precipitation time series X_t and the influencing factor Z_t, resulting in the updated time series W_t and F_t. These time series are discretized into five equidistant intervals to reduce the impact of noise while capturing a wider range of time series values across various magnitudes. Notably, the division into five equidistant boxes is a deduced outcome derived from rigorous comparative analyses and verifications (Franzen et al., 2020).

Step 2: Calculate the probability distribution functions for the time series:

$$\begin{cases} p(q_i) = \dfrac{\mathrm{count}(q_i)}{n} \\ p(w_j) = \dfrac{\mathrm{count}(w_j)}{n} \\ p(f_k) = \dfrac{\mathrm{count}(f_k)}{n} \end{cases} \tag{15}$$

where $p(q_i)$, $p(w_j)$ and $p(f_k)$ are the probability distribution functions of Q_t, W_t and F_t respectively; $\mathrm{count}(q_i)$, $\mathrm{count}(w_j)$ and $\mathrm{count}(f_k)$ represent the occurrences of numerical values in Q_t, W_t and F_t, respectively; $i = 1, 2, \cdots, 5$; $j = 1, 2, \cdots, 5$; $k = 1, 2, \cdots, 5$.

Step 3: The Shannon entropy of time series is calculated as follows:

$$H(Q_t) = -\sum_{i=1}^{5} p(q_i) \log_2 p(q_i) \tag{16}$$

where $H(Q_t)$ is the Shannon entropy of Q_t. Here, entropy with a logarithm of base 2 is considered, such that entropy and related IT measures are in units of bits.

Step 4: Calculate the joint distribution functions as follows:

$$\begin{cases} p(q_i, f_k) = \dfrac{\mathrm{count}(Q_t = q_i, F_t = f_k)}{n} \\ p(q_i, w_j) = \dfrac{\mathrm{count}(Q_t = q_i, W_t = w_j)}{n} \end{cases} \tag{17}$$

where $p(q_i, f_k)$ is the joint distribution function of Q_t and F_t; $p(q_i, w_j)$ is the joint distribution function of Q_t and W_t; $\mathrm{count}(Q_t = q_i, F_t = f_k)$ is the number of simultaneous occurrences of $Q_t = q_i$ and $F_t = f_k$; $\mathrm{count}(Q_t = q_i, W_t = w_j)$ is the number of simultaneous occurrences of $Q_t = q_i$ and

$W_t = w_j$.

Step 5: Given the influencing factor, the quantification of uncertainty within the sequence becomes feasible through the utilization of conditional entropy. This measure is computed as follows:

$$\begin{cases} H(Q_t|F_t) = \sum_{i=1}^{5}\sum_{k=1}^{5} p(q_i,f_k)\log_2\dfrac{p(q_i,f_k)}{p(f_k)} \\ H(Q_t|W_t) = \sum_{i=1}^{5}\sum_{j=1}^{5} p(q_i,w_j)\log_2\dfrac{p(q_i,w_j)}{p(w_j)} \end{cases} \tag{18}$$

where $H(Q_t|F_t)$ is the conditional entropy of Q_t given F_t; $H(Q_t|W_t)$ is the conditional entropy of Q_t given W_t.

Step 6: Mutual information $I(Q_t;F_t)$, quantifies the reduction in uncertainty of one variable when another variable is known. It is the difference between entropy and conditional entropy. The calculation for mutual information is as follows:

$$I(Q_t;F_t) = H(Q_t) - H(Q_t|F_t) = \sum p(q_t,f_t)\log_2\frac{p(q_t,f_t)}{p(q_t)p(f_t)} \tag{19}$$

Step 7: The DPRL index is further updated as follows:

$$\mathrm{DPRL}(t) = \frac{I(Q_t;F_t)}{H(Q_t|W_t)+1} \tag{20}$$

where $I(Q_t;F_t)$ represents the mutual information between Q_t and F_t. It quantifies the reduction in the uncertainty of Q_t when F_t is given, providing insights into their interdependence. With regard to the impact of precipitation on runoff, this index introduces the concept of conditional entropy $H(Q_t|W_t)$, accounting for the conditional uncertainty within runoff given precipitation. Furthermore, incorporating the notion of relative error, a modification is applied to the denominator by adding + 1. This adjustment prevents the denominator from becoming exceedingly small, which may lead to anomalous metric values of the index.

According to the aforementioned formulas derivation, the enhancements of the DPRS and DPRL indices are summarized. (1) Compared to conventional hydrological models, the DPRS and DPRL indices have lower data requirements and offer a simple and effective technique for identifying the possible impacts of driving factors on PPR. They also address the limitations of process-driven hydrological models in the run, which assume stationary and linear conditions (Ammann et al., 2019; Jehanzaib et al., 2020). (2) DPRS overcomes nonstationary effects by subtracting the local trend with appropriate polynomial orders, ensuring the normality of input signals for cross-correlation analysis (Zebende, 2011). (3) The effect of external factors on PPR may lead to spurious cross-correlation estimations (Yuan et al., 2015). Hence, the DPRL reveals intrinsic relationships between precipitation and runoff time series by excluding the influence of external factors, such as evapotranspiration, groundwater, land cover, and anthropogenic interference. (4) DPRL quantifies the nonlinear nature of the precipitation-runoff links and their associated driving factors. (5) DPRS elucidates possible driving mechanisms affecting PPR at various time scales, which can improve our understanding of hydrological responses to climate forcing and anthropogenic activities at various time scales. Within a specified period, the driving direction of DPRS signifies the influence exerted by a particular factor on the correlation between precipitation and runoff during the period. It is imperative to note that DPRS is constructed utilizing DCCA and DPCCA. DPRS solely captures the driving level and direction of influencing factors in the changes of PPR but does not represent the specific water quantity behaviors in the hydrological cycle. (6) The DPRS and DPRL indices provide the driving levels and allow for comparisons of the index values among different driving factors with inconsistent data-sequence lengths and across various types of catchments. (7) Indeed, DCCA and DPCCA can only capture the PRR at various time scales (Yuan et al., 2015). Therefore, the kernel density function is applied to the DPRS index to provide a definitive value for exploring the possible processes controls of PRR. (8) Baseflow, which plays a crucial role in the PRR, is subjected to a pre-processing step involving the determination of the time lag between precipitation and the mass centers of baseflow (Singh, 1968). This pre-processing step is performed prior to the application of the DPRS, allowing for a more accurate analysis of the possible driver of the changes in PRR. (9) The uncertainty was associated with driving factors (such as climate forcing, groundwater, vegetation dynamics, and anthropogenic influences) influencing the PRR across various time scales, characterized by violin plots. To illustrate, consider the influence of vegetation dynamics: on shorter time scales, vegetation's effect on runoff is markedly seasonal. During the growth period, an increase in leaf area can intercept precipitation and elevate transpiration rates, consequently reducing runoff (Gaertner et al., 2019). Conversely, in the dormant period, a reduction in vegetation cover can result in increased runoff. On broader time scales, land-use changes such as deforestation or afforestation exert enduring effects on runoff patterns. Specifically, deforestation can increase runoff by diminishing precipitation interception and transpiration, whereas afforestation may boost groundwater recharge and diminish runoff (Krishnaswamy et al., 2018). All related explanations will be clarified in the revised manuscript. Violin plot combines features of box plots and density plots to display data distribution. The wider sections of the violin plot indicate a higher probability of data distribution, whereas the narrower sections suggest a lower probability (Hintze and Nelson, 1998). Therefore, given the same volume of data, a vertically flatter or multimodal violin plot signifies a lower concentration and higher uncertainty of driving levels for the changes in the PRR as the time scale changes (if you have interest in codes, please do not hesitate to contact us).

4. Results

4.1. Precipitation-runoff relationships in study cases

The monthly precipitation-runoff correlation of five sub-basins in the Wei River Basin was examined using Detrended Cross-Correlation Analysis (DCCA), as depicted in Fig. 4a. The DCCA results indicated that WRB2 and WRB3 exhibited the strongest precipitation-runoff correlation, with PRR values concentrated around 0.8 and 0.87, respectively. WRB1 and WRB4 displayed lower PRR values, centered around 0.6. WRB5 exhibited the lowest PRR value, approximately 0.5. Examining the PRR results of these five sub-basins, WRB5 showed the highest uncertainty, while WRB1 and WRB4 displayed lower uncertainty. WRB2 and WRB3 exhibited the lowest uncertainty. The variability in PRR values across the sub-basins is attributed to the natural geographic conditions and anthropogenic factors within each sub-basin. WRB1, located in the upstream region of the Wei River Basin with a sparse population, experiences minimal anthropogenic influence. WRB4 and WRB5, situated in the downstream tributaries of the Wei River Basin in the semi-arid loess plateau region, are significantly impacted by afforestation policies, resulting in dynamic vegetation changes. WRB2 and WRB3, located in the upper to middle reaches of the Wei River Basin, are densely populated urban areas along the river, experiencing the greatest anthropogenic influence. Possible driving mechanisms for these results are provided in Sections 4.2 and 4.3.

4.2. Possible driving mechanisms in precipitation-runoff relationships with nonstationary theory approach

DPRS was utilized to quantify the driving levels and directions of possible influencing factors in the precipitation-runoff relationships under nonstationary conditions. The absolute values of the DPRS results (Fig. 4c) as well as the maximum kernel density values (Fig. 4d) were employed for comparing the levels of the driving forces associated with possible influencing factors. The results illustrate that the DPRS values

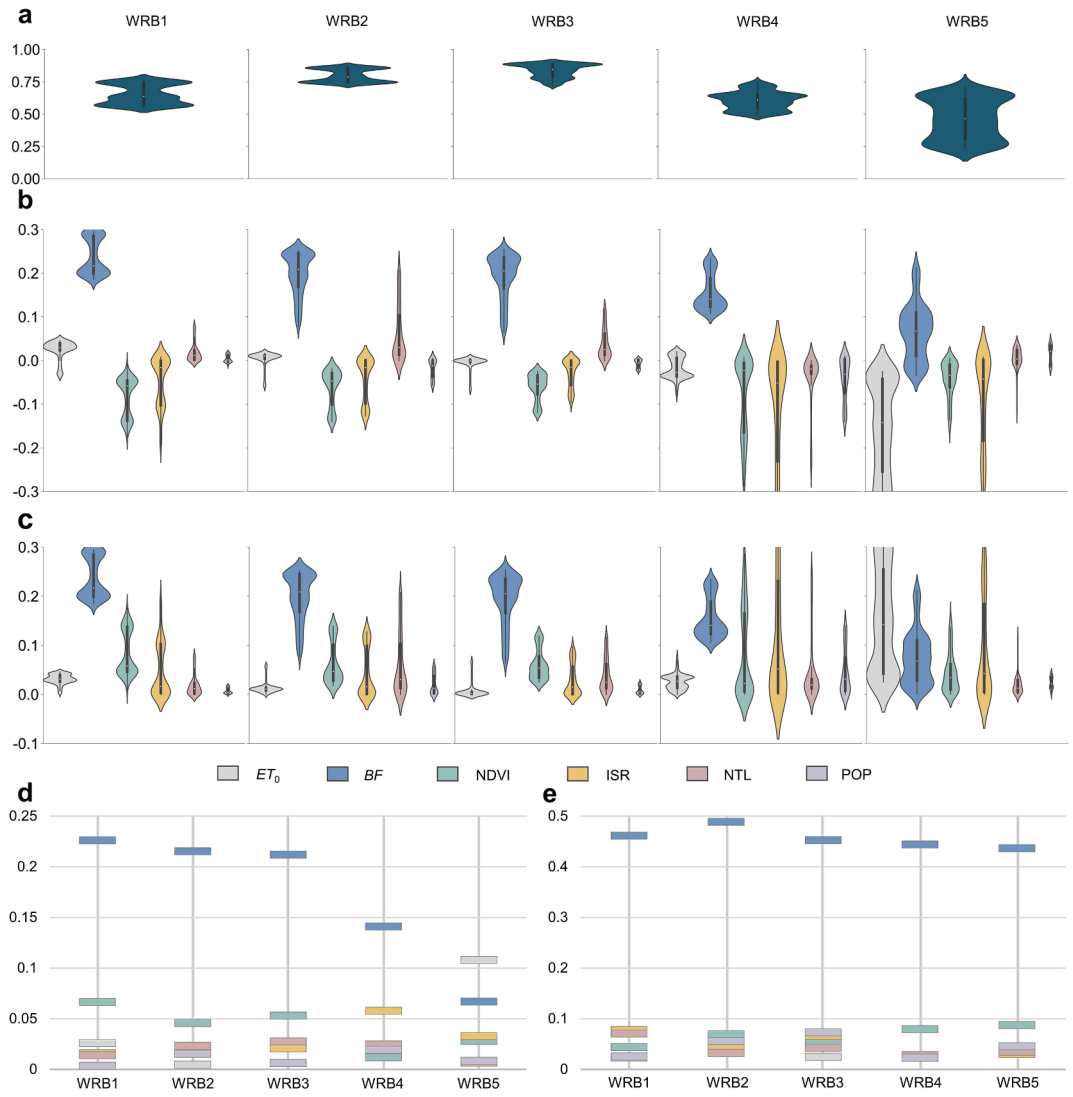

Fig. 4. A, precipitation-runoff relationships of five sub-basins within the wei river basin under nonstationary hydrological processes, investigated using dcca values. b, driving levels and directions of possible influencing factors in changes of precipitation-runoff relationships within the wei river basin, as indicated by dprs values. c, absolute values of dprs for possible influencing factors. d, Maximum kernel density values of the absolute values of DPRS for possible influencing factors. e, Values of DPRL for possible influencing factors.

of baseflow in WRB1, WRB2, WRB3, and WRB4 significantly exceeded those of other factors, while in WRB5, baseflow's DPRS values ranked second. This phenomenon indicates baseflow has a dominant influence on PRR. These findings align with the current dominance of groundwater in the hydrological cycle of the Wei River Basin. The five sub-basins are located in a continental monsoon climate region characterized by abundant rainfall in summer and limited precipitation in winter, where baseflow constitutes a substantial portion of the annual runoff. During the dry season, evaporation and percolation processes lead to a reduction in soil moisture. Precipitation replenishes soil moisture through the infiltration process, further contributing to baseflow. Concurrently, the soil's absorption of precipitation reduces surface runoff, making baseflow a primary component of runoff (Miao et al., 2020). On the other hand, depending on soil properties, the flow velocity of baseflow may be considerably lower than surface runoff, resulting in groundwater recharge during the wet season becoming the primary source of baseflow during the dry season (Huang et al., 2020). Furthermore, the DPRS values in the five sub-basins exhibit significant uncertainty. This is closely related to diverse factors within the study cases, such as groundwater depth, groundwater extraction, and urban development. Firstly, the diversity in groundwater depth impacts the flow velocity of baseflow, subsequently influencing the response time of runoff to precipitation. Secondly, groundwater extraction leads to reduced groundwater storage and lowered water tables, diminishing the generation of baseflow, reducing its flow velocity, and leading to varied responses of runoff to precipitation. Lastly, urban expansion has increased impervious surfaces, complicating soil properties. The development of urban clusters is accompanied by an increase in water demand, prompting the redistribution and utilization of water resources, such as reservoir construction and interregional water transfer, which significantly impact the regional PRR (Huang et al., 2017a).

The DPRS results of NDVI show that vegetation dynamics have negative impacts on the PRR in all five sub-basins. In WRB1, WRB2, and WRB3, the influence of vegetation dynamics on the PRR is secondary only to baseflow, with lower uncertainty compared to baseflow. Changes in vegetation cover primarily affect regional evapotranspiration. An increase in vegetation coverage leads to increased water consumption through regional vegetation transpiration, resulting in a decrease in soil moisture and ultimately affecting the migration speed of groundwater and reducing baseflow generation. When soil moisture levels are low and precipitation events occur, incoming precipitation infiltrates into the soil, reducing surface runoff (Buechel et al., 2022).

Additionally, vegetation intercepts surface runoff, prolonging the concentration time of surface runoff and increasing soil infiltration. However, the additional infiltration from interception is less compared to the water losses due to evaporation. WRB1 is situated in the upstream source area of the Wei River Basin, where precipitation is relatively lower than in other sub-basins. In WRB1, vegetation interception of low-intensity precipitation events greatly impacts the PRR. With rapid economic development, there has been an increasing awareness of ecological conservation. Since the 1950 s, soil and water conservation projects in the Wei River Basin have been continuously promoted, leading to a consistent increase in vegetation coverage across sub-basins (Chang et al., 2015). However, in WRB2 and WRB3, rapid urban expansion has diminished the impact of vegetation protection. Simultaneously, extensive human activities have introduced complex effects of vegetation dynamics on PRR. In WRB4 and WRB5, the influence of vegetation dynamics is smaller, but it exhibits higher uncertainty, especially in WRB4. Different forms of vegetation cover growth are a crucial factor contributing to this difference. In planned green areas within urban and *peri*-urban regions, vegetation is often transplanted from other areas. This greening approach leads to a rapid response of PRR to vegetation cover changes. In non-urban areas, young plants are typically used for greening, which may take several years (depending on the vegetation type) to significantly impact PRR. Moreover, non-urban greening areas are usually larger, and phased construction may result in varying driving levels of vegetation dynamics on PRR. It is noteworthy that the impact of vegetation dynamics on PRR in WRB4 is lower than in WRB5. The successful implementation of afforestation policies in WRB5 is a key factor explaining this phenomenon (Wu et al., 2023).

In the five sub-basins, ET_0 has both positive and negative effects on PRR. The complex behaviors are related to the mechanisms influencing ET_0. Evapotranspiration is the process by which water transforms from a liquid to a gaseous state, and it is influenced by energy and environmental factors. Meteorological factors such as temperature, humidity, and wind speed all have potential control over the evaporation process, thus affecting the magnitude of potential evapotranspiration. Global climate change and human interventions have led to intricate variations in meteorological elements. Consequently, the impact of ET_0 on the PRR exhibits diverse and intricate characteristics. ET_0 has the greatest influence on PRR in WRB5, showing significant uncertainty, while its impact in other sub-basins is small (Fig. 4c). This could be attributed to periodic vegetation changes within the sub-basins affecting local climate and subsequently influencing the PRR within the sub-basins (Mu et al., 2007). Urban development within WRB1, WRB2, WRB3, and WRB4 leads to increased impervious areas that intercept precipitation, and the presence of tall buildings affect wind speed and direction. These changes alter the response of runoff to precipitation. The urban heat island effect generated by urban development influences atmospheric circulation in urban and surrounding regions, significantly impacting regional PRR (Wai et al., 2017; Zhang et al., 2020). Additionally, ET_0 is closely linked to irrigation zone management (Berghuijs et al., 2017; Tu et al., 2023). In WRB2, WRB3, and WRB5, numerous large-scale irrigation zones have been established (Fig. 1c). Groundwater, river flow, vegetation cover, and infiltration processes within the sub-basins are all influenced by the operation of these irrigation zones, resulting in changes in PRR within the sub-basins.

ISR, NTL, and POP are specific manifestations of human activities. These three factors have both direct and indirect impacts on the runoff generation process, making their influence on the PRR complex. ISR is a direct indicator of urban expansion (Gong et al., 2020). Compared to NTL and POP, ISR has a stronger direct reduction effect on precipitation-runoff dependency within the sub-basins (Fig. 4b). In WRB4, the impact of ISR ranks second only to baseflow, while in other sub-basins, ISR also exerts a significant influence on PRR. The high impact of ISR on PRR is due to impervious areas directly intercepting precipitation at the ground surface, obstructing soil evaporation and infiltration processes. During precipitation events, larger impervious surfaces increase surface runoff generation, shorten concentration times, and induce flooding. Reduced soil evaporation ensures that the soil retains more moisture, leading to increased baseflow, although this is outweighed by the losses resulting from obstructed infiltration processes. Since the effects of impervious surfaces tend to stabilize once they are established, the impact of ISR on PRR remains consistent. In contrast to the direct impact of ISR on PRR, the influence of NTL and POP is mostly indirect. Aside from WRB4, where NTL exhibits a negative impact on PRR, it shows positive effects in other sub-basins (Fig. 4b). NTL exhibits an increasing trend with economic development, reflecting higher energy consumption levels (Liao et al., 2017). Along with energy consumption, energy release leads to the urban heat island effect, which affects regional precipitation, temperature, and meteorological elements. POP has various impacts on runoff formation, primarily related to water consumption. WRB1 has a smaller population, resulting in a minor influence on PRR. WRB5, although also sparsely populated, features reservoirs such as Tuojiahe Reservoir and Zhengjiahe Reservoir (Fig. 1b), diverting water resources to other areas, and affecting PRR within WRB5. Due to larger populations, POP exhibits stronger driving forces in WRB2 and WRB4. Notably, WRB3 has the highest population among the five sub-basins, but the driving level of POP is low. It is inferred that water transfer projects have alleviated the pressure of local water consumption on water resources in WRB3 (Zhang et al., 2011a). In summary, ISR primarily has a negative impact on PRR. In comparison to ISR across the five sub-basins, NTL and POP exert relatively weaker overall driving forces, primarily resulting in indirect impacts on PRR. However, the assessment of POP's influence on the PRR is limited due to the constraints of the time series length.

4.3. *Possible driving mechanisms in precipitation-runoff relationships with nonlinear theory approach*

DPRL applies the mutual information technique to quantitatively assess the driving levels of possible influencing factors in the precipitation-runoff relationships within the complex nonlinear hydrological processes. The results (Fig. 4e) illustrate that baseflow is the primary driving force influencing the PRR in the five sub-basins. The DPRL values of baseflow are all greater than 0.4 in the five sub-basins, while the DPRL values of other factors are all below 0.1. Baseflow is an important component of the Wei River Basin's runoff, particularly during the dry season (Miao et al., 2020), primarily contributing to runoff generation. Therefore, the DPRL values of baseflow are higher. The impact of vegetation dynamics in WRB4 and WRB5 is stronger than in other sub-basins and significantly exceeds the impact of other factors in the two sub-basins. The finding aligns with the lower level of urbanization in WRB4 and WRB5. Furthermore, the impact of vegetation dynamics in WRB5 is greater than in WRB4, illustrating that the afforestation policy in WRB5 has yielded positive results (Wu et al., 2023). Additionally, compared to WRB2, WRB3 has a higher proportion of irrigated areas, and the typical cropping pattern in these sub-basins includes winter wheat and summer maize. The vegetation dynamics within irrigation zones depend on changes in cropping patterns, thereby exerting complex effects on the PRR within the sub-basins. The impacts of ISR, NTL, and POP in WRB3 are all in the top two levels, and their impacts in WRB2 are slightly smaller than those in WRB3. Conversely, the impact of vegetation dynamics in WRB2 is greater than that in WRB3. The rapid expansion of downstream urban clusters in WRB3 is a significant factor contributing to this result. Simultaneously, in pursuit of higher economic income or a more convenient lifestyle, populations in WRB4 and WRB5 tend to migrate towards the central cities in WRB3. This migration results in lower anthropogenic driving factors for PRR in WRB4 and WRB5. Additionally, as populations concentrate, local surface water resources become inadequate to meet regional water demands. Consequently, groundwater extraction and inter-basin water transfer are employed to alleviate water resource pressures, leading to complex artificial interventions that may impact the PRR. ET_0 has a

smaller impact on the PRR in all five sub-basins. The ranking pattern of DPRL values of ET_0 in the sub-basins is similar to that of vegetation dynamics. ISR and NTL have the strongest impact in WRB1, likely due to its being the smallest basin area. Notably, the similar possible driving mechanisms are elaborated in greater detail in Section 4.2 and are not reiterated here.

4.4. Mutual validation of nonstationary and nonlinear theory approach outcomes

The patterns exhibited by DPRS and DPRL in Sections 4.2 and 4.3 are generally consistent, which mutually validates the reliability of their assessment outcomes. Both DPRS and DPRL results illustrate that baseflow is the primary factor influencing PRR. Excluding WRB5, the DPRS values of baseflow are the highest among the six factors. In WRB5, the DPRS value of baseflow ranks second only to ET_0. The DPRL values of baseflow are significantly higher than those of other factors in all five sub-basins. Furthermore, the DPRS and DPRL results for ISR, NTL, and POP demonstrate the differences between WRB2 and WRB3. WRB2 is located upstream of WRB3 and there is a large urban cluster downstream of WRB3. Therefore, ISR, NTL, and POP have a greater impact on PRR in WRB3 compared to WRB2. In contrast, WRB4 and WRB5 have smaller urban areas, so vegetation dynamics exhibit positive impacts in DPRS results and high-level influence in DPRL results. However, due to the distinct foundations of DPRS and DPRL, which are based on nonstationary and nonlinear theories, respectively. Their results exhibit minor disparities. For instance, in WRB5, the results from DPRS show that ET_0 has a much higher impact on PRR than other factors, whereas in DPRL results, the driving level of ET_0 is extremely low, almost equal to other factors. This disparity might be attributed to the implementation of afforestation policies in WRB5, which altered the local climate, thereby causing an increase in the driving level of ET_0 on PRR during specific periods. DPRS captures the influence of ET_0 on PRR (Fig. 4c), hence demonstrating a high driving level in the maximum kernel density results.

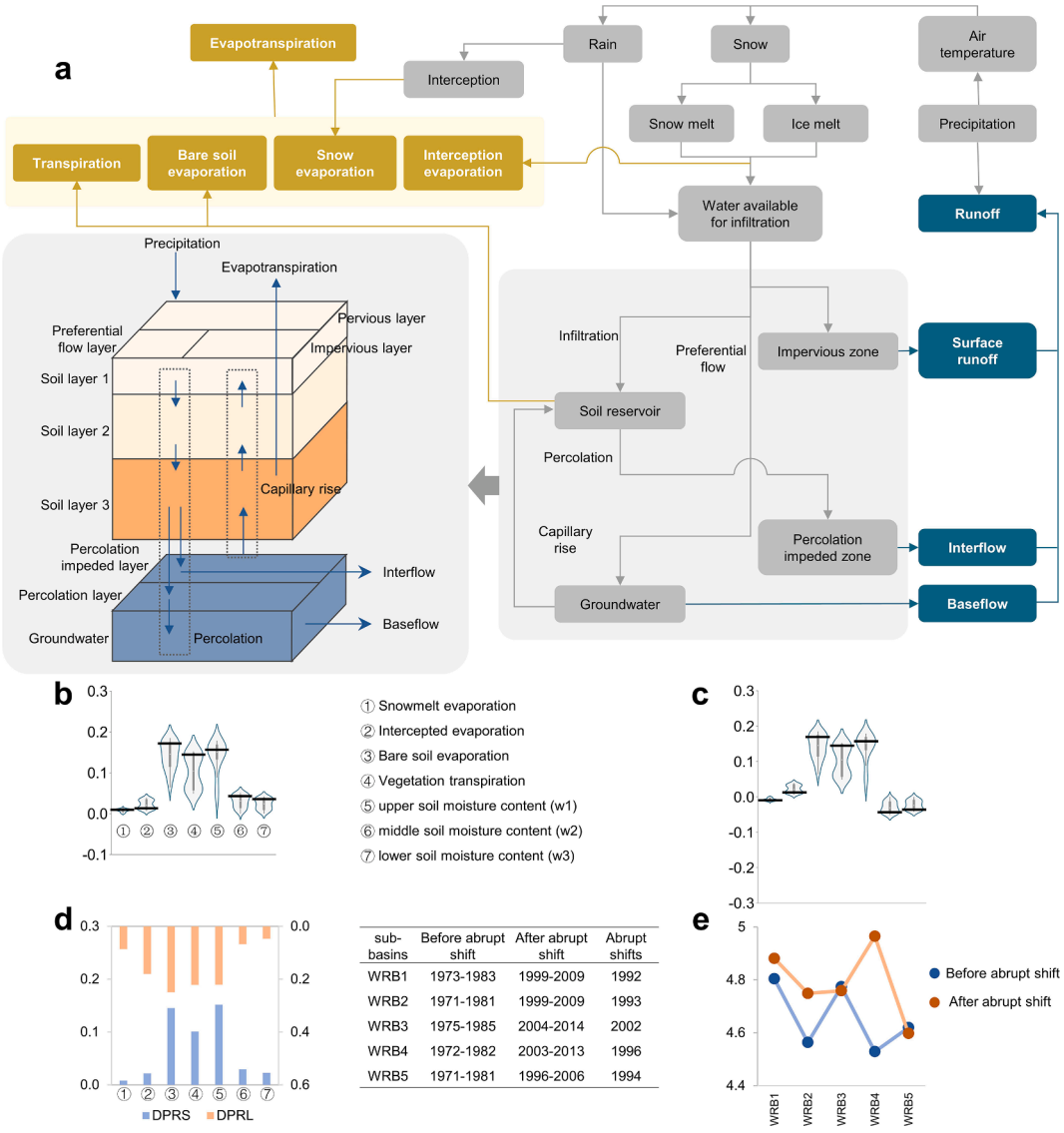

sub-basins	Before abrupt shift	After abrupt shift	Abrupt shifts
WRB1	1973-1983	1999-2009	1992
WRB2	1971-1981	1999-2009	1993
WRB3	1975-1985	2004-2014	2002
WRB4	1972-1982	2003-2013	1996
WRB5	1971-1981	1996-2006	1994

Fig. 5. a, Schematic overview of the CWatM framework for the hydrological processes with minimal anthropogenic influence. **b,** Driving levels of various land evapotranspiration and soil moisture content at different depths in changes of precipitation-runoff relationships within WRB1, as indicated by absolute values of DPRS values. **c,** Values of DPRS illustrating the driving direction. **d,** Maximum kernel density values of the absolute values of DPRS and DPRL values based on the results of various land evapotranspiration and soil moisture content at different depths in CWatM. **e,** Basin complexity results from five sub-basins before and after hydrological abrupt shifts considering nonstationary schemes.

5. Discussion

5.1. Application of the driving indices in a physically-based hydrological model

An in-depth analysis of the driving mechanisms of various land evapotranspiration (e.g., snowmelt evaporation, interception evaporation, bare soil evaporation, and vegetation transpiration) and soil moisture content at different depths in the precipitation-runoff relationships is performed by the employment of the DPRS and DPRL indices, using a high-resolution Community Water Model (CWatM).

5.1.1. Theory of physically-based hydrological model

The CWatM has a flexible modular structure and unique global and regional spatial representations. This section provides a case study of the Hulu River Basin at monthly time scale, under the control of the Qin'an hydrological monitoring station, focusing on the period from 1960 to 1978, which had minimal anthropogenic influence. The inputs for the model include observed streamflow data, meteorological data, and geographical information data (refer to Table S3 for specific details). Fig. 5a shows the schematic overview of the CWatM framework for the hydrological processes with minimal anthropogenic influence. The model employs diverse datasets of daily meteorological driving as inputs for Penman-Monteith calculations to estimate potential evapotranspiration. Precipitation is partitioned into rain and snow based on sub-grid elevation data and temperature. Water balance computations are conducted separately for six land cover classes (forest, irrigated, paddy-irrigated, water-covered, sealed area, and grassland). Four land cover classes (forest, irrigated, paddy-irrigated, and grassland) have separate calculations for soil processes, water interception, and evaporation of intercepted water. The resulting flux and storage for each grid cell are aggregated using the fraction of each land cover class within the grid cell. The model runs with preferential flow, which bypasses soil layers and percolates directly into groundwater. Soil moisture redistribution is estimated in three soil layers using the Van Genuchten simplification of the Richards equation. Direct evaporation from the soil surface is computed individually for two additional land cover classes, water and impermeable surfaces, while evaporation and runoff are calculated separately. Groundwater storage is modeled using a linear reservoir model. In addition, the information of inputs for the model, including dataset, duration, time and spatial resolution, and source, is shown in Table S3. The more detailed calculation principles for land evapotranspiration and soil moisture content are elaborated in Supporting Information S5.2. Model calibration and validation are illustrated in Supporting Information S5.3. Furthermore, in the hydrological model applied for the Hulu River Basin, while surface evaporation was accounted for, it was not identified as a primary driving factor for detailed exploration due to two main reasons. Firstly, the study area contains a limited number of grid cells classified as aquatic environments, with the vast majority representing terrestrial landscapes. Secondly, the evaporation from these water bodies leads to a direct decrease in runoff volumes, demonstrating a clear linear relationship and well-established driving mechanisms.

Hulu River Basin (WRB1) is situated in the Loess Plateau, characterized by diverse land cover types and high altitudes ranging from 1203 to 2908 m (Han et al., 2020). It primarily experiences infiltration into the groundwater system through piston flow, followed by preferential flow. A notable characteristic of this infiltration process is its prolonged duration, often exceeding ten years (Huang et al., 2013; Lin and Wei, 2006). To ensure a precise depiction of the initial-state groundwater storage and soil moisture content, a warm-up period, including the years 1960 to 1972, has been established. Subsequently, a calibration period of 1973–1976 and a validation period of 1977–1978 are set. The objective function employs the Nash efficiency coefficient (NSE) as the performance measure. The model run produces monthly NSE values of 0.80 in the calibration period and 0.63 in the validation period (see Figure S1).

5.1.2. Selected hydrological processes for precipitation-runoff relationships

The CWatM simulates the four types of land evapotranspiration, including snowmelt evaporation, intercepted evaporation, bare soil evaporation, and vegetation transpiration. Snowmelt evaporation refers to the evaporation from the runoff generated by melting ice and snow. It plays a significant role in hydrological processes within mountainous and cold regions or seasons, contributing to increased atmospheric moisture content, reduced snowmelt runoff, and local cooling effects. Intercepted evaporation involves the storage and subsequent evaporation of precipitation intercepted by vegetation canopies, thus reducing the amount of water reaching the land surface and influencing infiltration and surface runoff generation. Bare soil evaporation refers to the evaporation of water bodies directly from the land surface without the presence of vegetation or insulating layers. This process accelerates soil moisture loss, diminishes water storage capacity in the soil, affects precipitation infiltration and groundwater recharge, and reduces surface runoff generation. Vegetation transpiration represents the process through which plants absorb soil moisture and release it into the atmosphere. It directly impacts soil moisture content, thereby influencing local seepage processes and climate conditions. However, vegetation transpiration is also influenced by soil moisture availability. In summary, snowmelt evaporation, intercepted evaporation, bare soil evaporation, and vegetation transpiration exhibit distinct effects on hydrological processes, including surface runoff, soil moisture content, and groundwater recharge. Namely, they play a pivotal role in shaping the precipitation-runoff links.

The CWatM model employs a three-layer soil structure, which possesses an advantage in accurately calculating water percolation and facilitating a comprehensive understanding of this prolonged infiltration process. The soil structure in CWatM is a benefit for the Hulu River Basin, which is in the Loess Plateau with thick deposits of loess and poor soil permeability(Huang et al., 2013). This model allows for the examination of the distinct roles played by different soil layers in the hydrological cycle. For example, evaporation from bare soil reduces the moisture content in the upper soil layer, while both the upper and middle soil layers influence the infiltration process. Vegetation transpiration uniformly affects the moisture content of all three soil layers. In this regard, it is of significant importance to analyze the varying levels of soil moisture content in different layers and their impact on the PRR.

5.1.3. Possible driving mechanisms of selected hydrological processes in the precipitation-runoff relationships

As shown in Fig. 5b and c, the DPRS index reveals the force mechanisms of land evapotranspiration and soil moisture content at different depths on PRR. The results show that the bare soil evaporation, vegetation transpiration, and upper soil moisture content (w1) exhibit high and positive force levels on PRR. However, the force levels exhibit a higher level of uncertainty. Snowmelt evaporation, middle soil moisture content (w2), and lower soil moisture content (w3) display low and negative force levels on PRR. The intercepted evaporation exhibits a low and passive impact on PRR. Fig. 5d shows the DPRL measure of the impact of various land evapotranspiration and soil moisture content at different depths on PRR. Furthermore, to cross-validate with DPRL results, the maximum kernel density values of DPRS absolute values for different factors were computed. The results indicate that the primary driving factors responsible for the PRR, as revealed by the DPRL, are consistent with those of the DPRS results. DPRL values for bare soil evaporation, vegetation transpiration, and upper soil moisture content (w1) are significantly higher than those of the other four factors, aligning with the results of the DPRS results. The candidate mechanisms are investigated as follows. Hulu River Basin is situated in arid and semi-arid regions. In comparison to snowmelt evaporation and intercepted evaporation, bare soil evaporation and vegetation transpiration occur more frequently and contribute significantly to PRR due to their larger

evaporation rates. The moisture content of the upper soil, regulated by the mechanisms of bare soil evaporation and vegetation transpiration, undergoes pronounced seasonal and interannual variations that are intricately linked to both runoff generation and the dependence of precipitation on runoff. Conversely, the middle soil moisture content and the lower soil moisture content primarily contribute to subsurface runoff generation. Due to poor soil permeability, the interaction between surface runoff and subsurface runoff is rather limited, resulting in a lower impact of w2 and w3 on the PRR.

5.2. Verification of assessment results for the driving indices using basin complexity

Basin complexity is applied to further validate the assessment results for the DPRS and DPRL. The concept of basin complexity was characterized by learning statistical patterns from streamflow time series and quantifying the difficulty in predicting historically similar streamflow events (Pande and Moayeri, 2018). Basins are regarded as more complex when streamflow generation is more difficult to predict. A more intricate model is necessary to forecast hydrological processes in one basin with higher complexity. Basin complexity serves as a metric of the hydrological cycle's complexity and is associated with the PRR and its driving factors. A higher basin complexity suggests more intricate interconnections among the factors.

5.2.1. Theory of basin complexity

The *k* nearest neighbor model (Lall and Sharma, 1996; Sharma et al., 1997) is employed to compute the basin complexity (Pande and Moayeri, 2018), while the Vapnik-Chervonenkis (VC) generalized theory (Vapnik, 2006) is used to balance the performance and complexity of the *k* nearest neighbor model to obtain the most suitable *k* nearest neighbor model. The VC generalized theory is a statistical learning theory proposed by Vladimir Vapnik and Alexey Chervonenkis in the late 1960 s and early 1970 s. The theory provides a framework and tools for analyzing the generalization ability and error-bound properties of machine learning algorithms. VC dimension and generalization error are key concepts of the VC generalized theory. The VC dimension measures the complexity of the hypothesis space of a learning algorithm (Pande et al., 2009). In simple terms, the VC dimension is the size of the largest sample set that the learning algorithm can completely separate. A higher VC dimension indicates greater representational power of the learning algorithm but may also lead to overfitting. Generalization error is the error of the learning algorithm on new samples, that is, the error rate of the model learned by the learning algorithm from the training sample set on unseen samples. The VC inequality provides an upper bound estimate of the generalization error. The calculation method of the basin complexity is shown in Supporting Information S6.

5.2.2. Possible driving mechanisms considering the hydrological regime shifts using basin complexity

Basin complexity for five sub-basins before and after hydrological abrupt shifts is illustrated in Fig. 5e. It is noteworthy that the abrupt shifts in the Wei River Basin are primarily driven by human interventions. Basin complexity serves as a metric quantifying the intricacy of the hydrological cycle and denotes the extent of influence exerted by various factors in the runoff generation process within the basin. Stronger basin complexity indicates that various factors have a greater impact on the precipitation-runoff relationship. Examination of basin complexity results, as depicted in Fig. 5e, reveals that prior to the abrupt shift, the basin complexity of WRB1 and WRB3 is higher. Following the abrupt shifts, basin complexity increased for WRB1, WRB2, and WRB4, while experiencing a slight decrease for WRB3 and WRB5. Considering the overall basin complexity, WRB1, WRB2, and WRB3 demonstrated higher basin complexity, while WRB5 exhibited diminished basin complexity. The results of DCCA, illustrated in Fig. 4a, indicated strong PRR in WRB1, WRB2, and WRB3, contrasting with the weaker PRR observed in WRB5, thus confirming the findings. Moreover, examination of the DPRS, depicted in Fig. 4d, revealed that compared to other basins, WRB4 displayed a more uniform distribution of driving levels of driving factors affecting the PRR. This suggests that the hydrological cycle process in WRB4 is influenced by a broader kind of factors, consistent with the observed basin complexity. Furthermore, human activities have a significant impact on the basins, affecting topography, climatic conditions, vegetation cover, soil conditions, and groundwater availability. Consequently, anthropogenic factors represent a crucial driving force for changes in basin complexity. However, the influence of human activities is intricate, resulting in an overall increasing trend in basin complexity, with occasional periods of decline. Although the driving factors considered in this research may not encompass all factors influencing the basins, the investigation of the impacts of various factors on the PRR under nonstationary and nonlinear conditions across different time spans is essential. The analysis of the driving factors influencing the PRR holds guidance for the development of hydrological models under nonstationary and nonlinear conditions.

5.3. Limitations

Certain limitations are explicitly stated. (1) Due to the intricate interplay of climate forcing, groundwater, vegetation dynamics, and anthropogenic influences on catchments, as well as the challenges associated with data collection on anthropogenic activities, it may not comprehensively account for all-inclusive or exhaustive driving factors in the changes of the PRR. (2) The estimation of baseflow using the digital filtering method also presents certain limitations. Issues such as data noise and gaps can significantly impact the accuracy of the results. Furthermore, the selection of appropriate filter parameters involves subjectivity, potentially leading to divergent base flow estimates.

6. Conclusions

This study investigates the possible driving mechanisms for changing precipitation-runoff relationships (PRR) with nonstationary and nonlinear theory approaches. The novel indices, Driving indices for Precipitation-Runoff relationships within the nonStationary and nonLinear theory approach (DPRS and DPRL), provide valuable insights into the possible driving mechanisms of PRR in hydrological processes under nonstationary and nonlinear conditions, respectively. Through mutual verification of the results of DPRS and DPRL, coupled with a comparative analysis the findings in previous literature, possible explanations for PRR changes in the Wei River Basin were explored, focusing on climate forcing, groundwater, vegetation dynamics, and anthropogenic influences.

The application of DPRS and DPRL has revealed the significant impact of these factors across different sub-basins of the Wei River Basin. Specifically, baseflow emerged as a predominant factor affecting PRR, highlighting its sensitivity to hydrological shifts. Additionally, potential evapotranspiration plays a crucial role in driving negative PRR changes in specific sub-basins, indicating a weakening correlation between precipitation and runoff due to climatic variations.

Vegetation dynamics were identified as another crucial determinant negatively impacting PRR, even with lower uncertainty compared to other factors. This illustrates the intricate balance between natural processes and anthropogenic interventions in controlling hydrological responses. Anthropogenic influences, quantified through ISR, NTL, and POP, demonstrated varied driving levels, with ISR exhibiting the strongest direct impact on PRR, closely associated with urbanization processes.

The mutual validation of DPRS and DPRL indices confirmed the significant interplay of these factors, with the dominance of baseflow and the significant contributions of urbanization and afforestation policies to the PRR dynamics within the basin. This research not only advances our understanding of the complex interactions controlling

hydrological processes but also provides a comprehensive analytical tool for assessing the impact of nonstationary and nonlinear factors on PRR.

Furthermore, by employing a physically-based hydrological model, this study extended the utility of the proposed framework to driving mechanisms governing various land evapotranspiration and soil moisture content at different depths in the PRR. The application of basin complexity as a metric for hydrological cycle complexity provided additional insights to validate the assessment outcomes for the DPRS and DPRL.

This study contributes to the body of knowledge on hydrological modeling and management, offering a comprehensive framework for analyzing the driving mechanisms behind PRR under the influence of nonstationary and nonlinear hydrological processes. These insights facilitate informed decision-making and sustainable water resource management strategies within the Wei River Basin and potentially other regions experiencing similar hydrological complexities.

CRediT authorship contribution statement

Tongfang Li: Conceptualization, Data curation, Methodology, Validation, Visualization, Writing – original draft. **Tian Lan:** Conceptualization, Data curation, Formal analysis, Funding acquisition, Methodology, Project administration, Resources, Validation, Writing – original draft. **Hongbo Zhang:** Conceptualization, Data curation, Project administration, Writing – review & editing. **Jing Sun:** Formal analysis, Writing – review & editing. **Chong-Yu Xu:** Project administration, Writing – review & editing. **Yongqin David Chen:** Project administration, Writing – review & editing.

Declaration of competing interest

The authors declare that they have no known competing financial interests or personal relationships that could have appeared to influence the work reported in this paper.

Data availability

Data will be made available on request.

Acknowledgments

This study is financially supported by the National Natural Science Foundation of China (NSFC) (Grant No. 52209006, and 52379003), the National Key R&D Program of China (2019YFC1510400), the China Postdoctoral Science Foundation (Grant No. 2021 M700018), the Fundamental Research Funds for the Central Universities, CHD (Grant No. 300102292104), and Research Council of Norway FRINATEK Project 274310.

Appendix A. Supplementary data

Supplementary data to this article can be found online at https://doi.org/10.1016/j.jhydrol.2024.131535.

References

Abbott, B.W., et al., 2019. Human domination of the global water cycle absent from depictions and perceptions. Nat. Geosci. 12 (7), 533–540. https://doi.org/10.1038/s41561-019-0374-y.

Aguiar, V., Guedes, I., 2015. Shannon entropy, Fisher information and uncertainty relations for log-periodic oscillators. Physica A 423, 72–79. https://doi.org/10.1016/j.physa.2014.12.031.

Ajami, H., et al., 2017. On the non-stationarity of hydrological response in anthropogenically unaffected catchments: an Australian perspective. Hydrol. Earth Syst. Sci. 21 (1), 281–294. https://doi.org/10.5194/hess-21-281-2017.

Ammann, L., Fenicia, F., Reichert, P., 2019. A likelihood framework for deterministic hydrological models and the importance of non-stationary autocorrelation. Hydrol. Earth Syst. Sci. 23 (4), 2147–2172. https://doi.org/10.5194/hess-23-2147-2019.

Armstrong, R.A., 2019. Should Pearson's correlation coefficient be avoided? Ophthal. Physl. Opt. 39 (5), 316–327. https://doi.org/10.1111/opo.12636.

Bai, P., Liu, X., Zhang, Y., Liu, C., 2020. Assessing the impacts of vegetation greenness change on evapotranspiration and water yield in China. Water Resour. Res. 56 (10), e2019W–R027019. https://doi.org/10.1029/2019WR027019.

Bales, R.C., et al., 2018. Mechanisms controlling the impact of multi-year drought on mountain hydrology. Sci. Rep. 8 (1), 690. https://doi.org/10.1038/s41598-017-19007-0.

Berghuijs, W.R., Larsen, J.R., van Emmerik, T.H.M., Woods, R.A., 2017. A global assessment of runoff sensitivity to changes in precipitation, potential evaporation, and other factors. Water Resour. Res. 53 (10), 8475–8486. https://doi.org/10.1002/2017WR021593.

Bouaziz, L., et al., 2018. Redressing the balance: quantifying net intercatchment groundwater flows. Hydrol. Earth Syst. Sci. 22 (12), 6415–6434. https://doi.org/10.5194/hess-22-6415-2018.

Brunsell, N.A., 2010. A multiscale information theory approach to assess spatial–temporal variability of daily precipitation. J. Hydrol. 385 (1), 165–172. https://doi.org/10.1016/j.jhydrol.2010.02.016.

Buechel, M., Slater, L., Dadson, S., 2022. Hydrological impact of widespread afforestation in Great Britain using a large ensemble of modelled scenarios. Commun. Earth Environ. 3 (1), 6. https://doi.org/10.1038/s43247-021-00334-0.

Carlier, C., Wirth, S.B., Cochand, F., Hunkeler, D., Brunner, P., 2018. Geology controls streamflow dynamics. J. Hydrol. 566, 756–769. https://doi.org/10.1016/j.jhydrol.2018.08.069.

Ceola, S., Laio, F., Montanari, A., 2014. Satellite nighttime lights reveal increasing human exposure to floods worldwide. Geophys. Res. Lett. 41 (20), 7184–7190. https://doi.org/10.1002/2014GL061859.

Ceola, S., Laio, F., Montanari, A., 2019. Global-scale human pressure evolution imprints on sustainability of river systems. Hydrol. Earth Syst. Sci. 23 (9), 3933–3944. https://doi.org/10.5194/hess-23-3933-2019.

Chang, J., et al., 2015. Impact of climate change and human activities on runoff in the Weihe River Basin. China. Quatern. Int. 380–381, 169–179. https://doi.org/10.1016/j.quaint.2014.03.048.

Chen, X.Z., et al., 2016. Detecting significant decreasing trends of land surface soil moisture in eastern China during the past three decades (1979–2010). J. Geophys. Res. Atmos. 121 (10), 5177–5192. https://doi.org/10.1002/2015jd024676.

Chen, L., Wei, W., Fu, B., Lü, Y., 2007. Soil and water conservation on the Loess Plateau in China: review and perspective. Prog. Phys. Geog. 31 (4), 389–403. https://doi.org/10.1177/0309133307081290.

Cover, T.M., 1999. Elements of information theory. John Wiley & Sons.

Cryer, J.D., Kellet, N., 1991. Time series analysis. Springer.

Dey, P., Mishra, A., 2017. Separating the impacts of climate change and human activities on streamflow: A review of methodologies and critical assumptions. J. Hydrol. 548, 278–290. https://doi.org/10.1016/j.jhydrol.2017.03.014.

Elvidge, C.D., et al., 2007. Global distribution and density of constructed impervious surfaces. Sensors 7 (9), 1962–1979. https://doi.org/10.3390/s7091962.

Fang, Y., Jawitz, J.W., 2019. The evolution of human population distance to water in the USA from 1790 to 2010. Nat. Commun. 10 (1), 430. https://doi.org/10.1038/s41467-019-08366-z.

Feng, X., Cheng, W., Fu, B., Lü, Y., 2016. The role of climatic and anthropogenic stresses on long-term runoff reduction from the Loess Plateau. China. Sci. Total Environ. 571, 688–698. https://doi.org/10.1016/j.scitotenv.2016.07.038.

Ficklin, D.L., Stewart, I.T., Maurer, E.P., 2013. Climate change impacts on streamflow and subbasin-scale hydrology in the Upper Colorado River Basin. PLoS One 8 (8), e71297.

Fowler, K., et al., 2020. Many commonly used rainfall-runoff models lack long, slow dynamics: Implications for runoff projections. Water Resour. Res. 56 (5), e2019W–R025286. https://doi.org/10.1029/2019WR025286.

Fowler, K., et al., 2022. Explaining changes in rainfall–runoff relationships during and after Australia's Millennium Drought: a community perspective. Hydrol. Earth Syst. Sci. 26 (23), 6073–6120. https://doi.org/10.5194/hess-26-6073-2022.

Franzen, S.E., Farahani, M.A., Goodwell, A.E., 2020. Information flows: Characterizing precipitation-streamflow dependencies in the Colorado headwaters with an information theory approach. Water Resour. Res. 56 (10), e2019W–R026133. https://doi.org/10.1029/2019WR026133.

Gaertner, B.A., Zegre, N., Warner, T., Fernandez, R., He, Y., Merriam, E.R., 2019. Climate, forest growing season, and evapotranspiration changes in the central Appalachian Mountains, USA. Sci. Total Environ. 650, 1371–1381. https://doi.org/10.1016/j.scitotenv.2018.09.129.

Gao, P., Geissen, V., Ritsema, C.J., Mu, X.M., Wang, F., 2013. Impact of climate change and anthropogenic activities on stream flow and sediment discharge in the Wei River basin. China. Hydrol. Earth Syst. Sci. 17 (3), 961–972. https://doi.org/10.5194/hess-17-961-2013.

Gong, P., et al., 2020. Annual maps of global artificial impervious area (GAIA) between 1985 and 2018. Remote Sens. Environ. 236, 111510 https://doi.org/10.1016/j.rse.2019.111510.

Goodwell, A.E., Jiang, P., Ruddell, B.L., Kumar, P., 2020. Debates—Does information theory provide a new paradigm for Earth science? Causality, interaction, and feedback. Water Resour. Res. 56 (2), e2019W–R024940. https://doi.org/10.1029/2019WR024940.

Gu, X., Zhang, Q., Singh, V.P., Xiao, M., Cheng, J., 2017. Nonstationarity-based evaluation of flood risk in the Pearl River basin: changing patterns, causes and implications. Hydrolog. Sci. J. 62 (2), 246–258. https://doi.org/10.1080/02626667.2016.1183774.

Han, H., et al., 2020. Impact of soil and water conservation measures and precipitation on streamflow in the middle and lower reaches of the Hulu River Basin. China. CATENA 195, 104792. https://doi.org/10.1016/j.catena.2020.104792.
Hare, D.K., Helton, A.M., Johnson, Z.C., Lane, J.W., Briggs, M.A., 2021. Continental-scale analysis of shallow and deep groundwater contributions to streams. Nat. Commun. 12 (1), 1450. https://doi.org/10.1038/s41467-021-21651-0.
Hejazi, M.I., Cai, X., 2009. Input variable selection for water resources systems using a modified minimum redundancy maximum relevance (mMRMR) algorithm. Adv. Water Resour. 32 (4), 582–593. https://doi.org/10.1016/j.advwatres.2009.01.009.
Hejazi, M.I., Cai, X., Ruddell, B.L., 2008. The role of hydrologic information in reservoir operation – Learning from historical releases. Adv. Water Resour. 31 (12), 1636–1650. https://doi.org/10.1016/j.advwatres.2008.07.013.
Hidalgo, H.G., et al., 2009. Detection and attribution of streamflow timing changes to climate change in the western United States. J. Climate 22 (13), 3838–3855. https://doi.org/10.1175/2009JCLI2470.1.
Hintze, J.L., Nelson, R.D., 1998. Violin plots: a box plot-density trace synergism. The American Statistician 52 (2), 181–184. https://doi.org/10.1080/00031305.1998.10480559.
Hirmas, D.R. et al., 2018. Climate-induced changes in continental-scale soil macroporosity may intensify water cycle. Nature, 561(7721): 100-103. Doi: 100-103, 10.1038/s41586-018-0463-x.
Hobbins, M., Senay, G., Gowda, P.H., Artan, G., 2016. Evapotranspiration and evaporative demand. Methods and Applications, Statistical Analysis of Hydrologic Variables, pp. 71–143.
Hobeichi, S., et al., 2022. Reconciling historical changes in the hydrological cycle over land. Npj Clim. Atmos. Sci. 5 (1), 17. https://doi.org/10.1038/s41612-022-00240-y.
Huang, X.-D., et al., 2020. Spatial patterns in baseflow mean response time across a watershed in the Loess Plateau: Linkage with land-use types. Forest Sci. 66 (3), 382–391. https://doi.org/10.1093/forsci/fxz084.
Huang, K., et al., 2021. Persistent increases in nighttime heat stress from urban expansion despite heat island mitigation. J. Geophys. Res-Atmos. 126 (4), e2020J–D033831. https://doi.org/10.1029/2020JD033831.
Huang, S., Chang, J., Huang, Q., Wang, Y., Chen, Y., 2014. Spatio-temporal changes in potential evaporation based on entropy across the Wei River Basin. Water Resour. Manag. 28 (13), 4599–4613. https://doi.org/10.1007/s11269-014-0760-6.
Huang, S., Huang, Q., Chang, J., Leng, G., Chen, Y., 2017a. Variations in precipitation and runoff from a multivariate perspective in the Wei River Basin. China. Quatern. Int. 440, 30–39. https://doi.org/10.1016/j.quaint.2016.05.020.
Huang, S.Z., Huang, Q., Leng, G.Y., Zhao, M.L., Meng, E., 2017b. Variations in annual water-energy balance and their correlations with vegetation and soil moisture dynamics: A case study in the Wei River Basin. China. J. Hydrol. 546, 515–525. https://doi.org/10.1016/j.jhydrol.2016.12.060.
Huang, T., Pang, Z., Yuan, L., 2013. Nitrate in groundwater and the unsaturated zone in (semi)arid northern China: baseline and factors controlling its transport and fate. Environ. Earth Sci. 70 (1), 145–156. https://doi.org/10.1007/s12665-012-2111-3.
Jehanzaib, M., Shah, S.A., Yoo, J., Kim, T.-W., 2020. Investigating the impacts of climate change and human activities on hydrological drought using non-stationary approaches. J. Hydrol. 588, 125052 https://doi.org/10.1016/j.jhydrol.2020.125052.
John, A., Nathan, R., Horne, A., Fowler, K., Stewardson, M., 2022. Nonstationary runoff responses can interact with climate change to increase severe outcomes for freshwater ecology. Water Resour. Res. 58 (2), e2021W–R030192. https://doi.org/10.1029/2021WR030192.
Kantelhardt, J.W., et al., 2002. Multifractal detrended fluctuation analysis of nonstationary time series. Physica A 316 (1), 87–114. https://doi.org/10.1016/S0378-4371(02)01383-3.
Kayitesi, N.M., Guzha, A.C., Mariethoz, G., 2022. Impacts of land use land cover change and climate change on river hydro-morphology- a review of research studies in tropical regions. J. Hydrol. 615, 128702 https://doi.org/10.1016/j.jhydrol.2022.128702.
Konapala, G., Mishra, A.K., Wada, Y., Mann, M.E., 2020. Climate change will affect global water availability through compounding changes in seasonal precipitation and evaporation. Nat. Commun. 11 (1), 3044. https://doi.org/10.1038/s41467-020-16757-w.
Krishnaswamy, J., Kelkar, N., Birkel, C., 2018. Positive and neutral effects of forest cover on dry-season stream flow in Costa Rica identified from Bayesian regression models with informative prior distributions. Hydrol. Process 32 (24), 3604–3614. https://doi.org/10.1002/hyp.13288.
Lall, U., Sharma, A., 1996. A nearest neighbor bootstrap for resampling hydrologic time series. Water Resour. Res. 32 (3), 679–693. https://doi.org/10.1029/95WR02966.
Lee, H., Verma, B., 2012. Binary segmentation algorithm for English cursive handwriting recognition. Pattern Recogn. 45 (4), 1306–1317. https://doi.org/10.1016/j.patcog.2011.09.015.
Liao, W., Liu, X., Wang, D., Sheng, Y., 2017. The impact of energy consumption on the surface urban heat island in China's 32 major cities. Remote Sens. 9 (3), 250.
Lin, C.-H., Ho, Y.K., 2015. Shannon information entropy in position space for two-electron atomic systems. Chem. Phys. Lett. 633, 261–264. https://doi.org/10.1016/j.cplett.2015.05.029.
Lin, R., Wei, K., 2006. Tritium profiles of pore water in the Chinese loess unsaturated zone: Implications for estimation of groundwater recharge. J. Hydrol. 328 (1), 192–199. https://doi.org/10.1016/j.jhydrol.2005.12.010.
Liu, J., et al., 2019. Global Attribution of Runoff Variance Across Multiple Timescales. J. Geophys. Res-Atmos. 124 (24), 13962–13974. https://doi.org/10.1029/2019JD030539.
Liu, D., Guo, S., Lian, Y., Xiong, L., Chen, X., 2015. Climate-informed low-flow frequency analysis using nonstationary modelling. Hydrol. Process. 29 (9), 2112–2124. https://doi.org/10.1002/hyp.10360.
Liu, Y., Yu, L., Chen, G., 2020. Characterization of sea surface temperature and air-sea heat flux anomalies associated with mesoscale eddies in the South China Sea. Journal of Geophysical Research: Oceans 125 (4), e2019J–C015470. https://doi.org/10.1029/2019JC015470.
Lu, M., et al., 2019. Effect of urbanisation on extreme precipitation based on nonstationary models in the Yangtze River Delta metropolitan region. Sci. Total Environ. 673, 64–73. https://doi.org/10.1016/j.scitotenv.2019.03.413.
Mekonnen, M.M., Hoekstra, A.Y., 2016. Four billion people facing severe water scarcity. Sci. Adv. 2 (2), e1500323.
Miao, C., et al., 2020. The changing relationship between rainfall and surface runoff on the Loess Plateau, China. J. Geophys. Res-Atmos. 125 (8), e2019J–D032053. https://doi.org/10.1029/2019JD032053.
Mishra, S., Ayyub, B.M., 2019. Shannon Entropy for quantifying uncertainty and risk in economic disparity. Risk Anal. 39 (10), 2160–2181. https://doi.org/10.1111/risa.13313.
Mishra, A.K., Özger, M., Singh, V.P., 2009. An entropy-based investigation into the variability of precipitation. J. Hydrol. 370 (1), 139–154. https://doi.org/10.1016/j.jhydrol.2009.03.006.
Mu, X., Zhang, L., McVicar, T.R., Chille, B., Gau, P., 2007. Analysis of the impact of conservation measures on stream flow regime in catchments of the Loess Plateau. China. Hydrol. Process. 21 (16), 2124–2134. https://doi.org/10.1002/hyp.6391.
Nayak, P.C., Venkatesh, B., Krishna, B., Jain, S.K., 2013. Rainfall-runoff modeling using conceptual, data driven, and wavelet based computing approach. J. Hydrol. 493, 57–67. https://doi.org/10.1016/j.jhydrol.2013.04.016.
Nourani, V., Khanghah, T.R., Baghanam, A.H., 2016. Application of entropy concept for input selection of Wavelet-ANN based rainfall-runoff modeling. J Environ. Inform. 26 (1), 52–70.
Pande, S., McKee, M., Bastidas, L.A., 2009. Complexity-based robust hydrologic prediction. Water Resour. Res. 45 (10) https://doi.org/10.1029/2008WR007524.
Pande, S., Moayeri, M., 2018. Hydrological interpretation of a statistical measure of basin complexity. Water Resour. Res. 54 (10), 7403–7416. https://doi.org/10.1029/2018WR022675.
Pathiraja, S., Marshall, L., Sharma, A., Moradkhani, H., 2016. Hydrologic modeling in dynamic catchments: A data assimilation approach. Water Resour. Res. 52 (5), 3350–3372. https://doi.org/10.1002/2015WR017192.
Pechlivanidis, I.G., Jackson, B., Mcmillan, H., Gupta, H.V., 2016. Robust informational entropy-based descriptors of flow in catchment hydrology. Hydrolog. Sci. J. 61 (1), 1–18.
Pedregosa, F., et al., 2011. Scikit-learn: Machine learning in Python. the. Journal of Machine Learning Research 12, 2825–2830.
Peng, C.K., et al., 1994. Mosaic organization of DNA nucleotides. Phys. Rev. E 49 (2), 1685–1689. https://doi.org/10.1103/PhysRevE.49.1685.
Perugini, D., et al., 2015. Quantifying magma mixing with the Shannon entropy: Application to simulations and experiments. Lithos 236–237, 299–310. https://doi.org/10.1016/j.lithos.2015.09.008.
Quinn, J.D., Reed, P.M., Giuliani, M., Castelletti, A., 2017. Rival framings: A framework for discovering how problem formulation uncertainties shape risk management trade-offs in water resources systems. Water Resour. Res. 53 (8), 7208–7233. https://doi.org/10.1002/2017WR020524.
Saft, M., Western, A.W., Zhang, L., Peel, M.C., Potter, N.J., 2015. The influence of multiyear drought on the annual rainfall-runoff relationship: An Australian perspective. Water Resour. Res. 51 (4), 2444–2463. https://doi.org/10.1002/2014WR015348.
Sang, Y.-F., Singh, V.P., Hu, Z., Xie, P., Li, X., 2018. Entropy-aided evaluation of meteorological droughts over China. J. Geophys. Res-Atmos. 123 (2), 740–749. https://doi.org/10.1002/2017JD026956.
Savenije, H.H.G., 1996. The runoff coefficient as the key to moisture recycling. J. Hydrol. 176 (1), 219–225. https://doi.org/10.1016/0022-1694(95)02776-9.
Shannon, C.E., 1948. A mathematical theory of communication. The Bell System Technical Journal 27 (3), 379–423. https://doi.org/10.1002/j.1538-7305.1948.tb01338.x.
Sharma, A., Tarboton, D.G., Lall, U., 1997. Streamflow simulation: A nonparametric approach. Water Resour. Res. 33 (2), 291–308. https://doi.org/10.1029/96WR02839.
Shuster, W.D., Bonta, J., Thurston, H., Warnemuende, E., Smith, D., 2005. Impacts of impervious surface on watershed hydrology: A review. Urban Water J. 2 (4), 263–275. https://doi.org/10.1080/15730620500386529.
Sikorska-Senoner, A.E., Quilty, J.M., 2021. A novel ensemble-based conceptual-data-driven approach for improved streamflow simulations. Environ. Modell. Softw. 143, 105094 https://doi.org/10.1016/j.envsoft.2021.105094.
Singh, K.P., 1968. Some factors affecting baseflow. Water Resour. Res. 4 (5), 985–999. https://doi.org/10.1029/WR004i005p00985.
Tarasova, L., Basso, S., Zink, M., Merz, R., 2018. Exploring controls on rainfall-runoff events: 1. Time series-based event separation and temporal dynamics of event runoff response in Germany. Water Resour. Res. 54 (10), 7711–7732. https://doi.org/10.1029/2018WR022587.
Thorslund, J., van Vliet, M.T.H., 2020. A global dataset of surface water and groundwater salinity measurements from 1980–2019. Sci. Data 7 (1), 231. https://doi.org/10.1038/s41597-020-0562-z.
Tu, Z., Yang, Y., Roderick, M.L., McVicar, T.R., 2023. Potential evaporation and the complementary relationship. Water Resour. Res. 59 (3), e2022W–R033763. https://doi.org/10.1029/2022WR033763.

Van Rensch, P., et al., 2023. The role of weather system changes and catchment characteristics in the rainfall-runoff relationship shift in Victoria, Australia. Water Resour. Res. 59 (6), e2022W–R033692. https://doi.org/10.1029/2022WR033692.
Vapnik, V., 2006. Estimation of dependences based on empirical data. Springer Science & Business Media.
Wai, K.M., et al., 2017. Observational evidence of a long-term increase in precipitation due to urbanization effects and its implications for sustainable urban living. Sci. Total Environ. 599–600, 647–654. https://doi.org/10.1016/j.scitotenv.2017.05.014.
Wang, Z., Xu, M., Liu, X., Singh, D.K., Fu, X., 2022. Quantifying the impact of climate change and anthropogenic activities on runoff and sediment load reduction in a typical Loess Plateau watershed. J. Hydrol. Regional Studies 39, 100992. https://doi.org/10.1016/j.ejrh.2022.100992.
Western, A.W., Grayson, R.B., Green, T.R., 1999. The Tarrawarra project: high resolution spatial measurement, modelling and analysis of soil moisture and hydrological response. Hydrol. Process. 13 (5), 633–652. https://doi.org/10.1002/(SICI)1099-1085(19990415)13:5<633::AID-HYP770>3.0.CO;2-8.
WorldPop, 2018. Global high resolution population denominators project. Funded by The Bill Melinda Gates Foundation (OPP1134076) Sch. Geogr. Environ. Sci. Univ. Southampton; Dep. Geogr. Geosci. Univ. Louisville; Departement de Geogr. Univ. de Namur) Cent. for Int. Earth Sci. Inf. Netw.(CIESIN), Columbia Univ.
Wu, Y., et al., 2013. Local Shannon entropy measure with statistical tests for image randomness. Inform. Sciences 222, 323–342. https://doi.org/10.1016/j.ins.2012.07.049.
Wu, C., et al., 2023. Effects of climate change and anthropogenic activities on runoff change of the Weihe River basin. Northwest China. River Res. Appl. 39 (4), 648–660. https://doi.org/10.1002/rra.4102.
Xie, T., Zhang, G., Hou, J., Xie, J., Lv, M., Liu, F., 2019. Hybrid forecasting model for non-stationary daily runoff series: a case study in the Han River Basin. China. J. Hydrol. 577, 123915 https://doi.org/10.1016/j.jhydrol.2019.123915.
Yang, T., et al., 2020. Comprehensive ecological risk assessment for semi-arid basin based on conceptual model of risk response and improved TOPSIS model-a case study of Wei River Basin. China. Sci. Total Environ. 719, 137502 https://doi.org/10.1016/j.scitotenv.2020.137502.
Yuan, N., et al., 2015. Detrended Partial-Cross-Correlation Analysis: A new method for analyzing correlations in complex system. Sci. Rep. 5 (1), 8143. https://doi.org/10.1038/srep08143.
Yue, S., Pilon, P., Phinney, B.O.B., 2003. Canadian streamflow trend detection: impacts of serial and cross-correlation. Hydrolog. Sci. J. 48 (1), 51–63. https://doi.org/10.1623/hysj.48.1.51.43478.
Yue, S., Wang, C., 2004. The Mann-Kendall Test Modified by Effective Sample Size to Detect Trend in Serially Correlated Hydrological Series. Water Resour. Manag. 18 (3), 201–218. https://doi.org/10.1023/B:WARM.0000043140.61082.60.
Zebende, G.F., 2011. DCCA cross-correlation coefficient: Quantifying level of cross-correlation. Physica A 390 (4), 614–618. https://doi.org/10.1016/j.physa.2010.10.022.
Zhan, C.S., et al., 2014. Quantitative contribution of climate change and human activities to runoff changes in the Wei River basin. China. Hydrol. Earth Syst. Sci. 18 (8), 3069–3077. https://doi.org/10.5194/hess-18-3069-2014.
Zhang, Z., et al., 2011b. Evaluating the non-stationary relationship between precipitation and streamflow in nine major basins of China during the past 50years. J. Hydrol. 409 (1), 81–93. https://doi.org/10.1016/j.jhydrol.2011.07.041.
Zhang, Y., et al., 2019. Human health risk assessment of groundwater arsenic contamination in Jinghui irrigation district. China. J. Environ. Manage. 237, 163–169. https://doi.org/10.1016/j.jenvman.2019.02.067.
Zhang, T., et al., 2022. Evaluation of the impacts of human activities on propagation from meteorological drought to hydrological drought in the Weihe River Basin. China. Sci. Total Environ. 819, 153030 https://doi.org/10.1016/j.scitotenv.2022.153030.
Zhang, L., Chen, X., Lai, R., 2020. Urban signatures of sub-daily extreme precipitation events over a metropolitan region. Atmos. Res. 246, 105204 https://doi.org/10.1016/j.atmosres.2020.105204.
Zhang, Y., Feng, X., Wang, X., Fu, B., 2018. Characterizing drought in terms of changes in the precipitation–runoff relationship: a case study of the Loess Plateau. China. Hydrol. Earth Syst. Sci. 22 (3), 1749–1766. https://doi.org/10.5194/hess-22-1749-2018.
Zhang, Q., Gu, X., Singh, V.P., Xiao, M., Chen, X., 2015. Evaluation of flood frequency under non-stationarity resulting from climate change and human activities in the East River basin. China. J. Hydrol. 527, 565–575. https://doi.org/10.1016/j.jhydrol.2015.05.029.
Zhang, Y., Jia, S., Huang, H., Qiu, J., Zhou, C., 2014. A novel algorithm for the precise calculation of the maximal information coefficient. Sci Rep 4 (1), 6662. https://doi.org/10.1038/srep06662.
Zhang, B., Sun, Y., Duan, L., Yang, S., 2011a. Effect of introducing Han River into Wei River on Wei River. In: 2011 International Symposium on Water Resource and Environmental Protection, pp. 1055–1058. https://doi.org/10.1109/ISWREP.2011.5893195.
Zhao, J., et al., 2015. Analysis of temporal and spatial trends of hydro-climatic variables in the Wei River Basin. Environ. Res. 139, 55–64. https://doi.org/10.1016/j.envres.2014.12.028.
Zuo, D., et al., 2015. Simulating spatiotemporal variability of blue and green water resources availability with uncertainty analysis. Hydrol. Process. 29 (8), 1942–1955. https://doi.org/10.1002/hyp.10307.
Zuo, D.P., Xu, Z.X., Yang, H., Liu, X.C., 2012. Spatiotemporal variations and abrupt changes of potential evapotranspiration and its sensitivity to key meteorological variables in the Wei River basin. China. Hydrol. Process. 26 (8), 1149–1160. https://doi.org/10.1002/hyp.8206.